ORIGINAL PAPER

Endoplasmic reticulum stress and mitochondrial injury are critical molecular drivers of AlCl₃-induced testicular and epididymal distortion and dysfunction: protective role of taurine

Hanaa A. Khalaf[1] · Ayman Z. Elsamanoudy[2,3] · Salwa M. Abo-Elkhair[2] · Fatma E. Hassan[4] · Passant M. Mohie[5] · Fatma M. Ghoneim[1]

Abstract

Aluminum, the third most plentiful metal in the Earth's crust, has potential for human exposure and harm. Oxidative stress plays an essential role in producing male infertility by inducing defects in sperm functions. We aimed to investigate the role of endoplasmic reticulum (ER) stress and mitochondrial injury in the pathogenesis of aluminum chloride (AlCl₃)-induced testicular and epididymal damage at the histological, biochemical, and molecular levels, and to assess the potential protective role of taurine. Forty-eight adult male albino rats were separated into four groups (12 in each): negative control, positive control, AlCl₃, and AlCl₃ plus taurine groups. Testes and epididymis were dissected. Histological and immunohistochemical (Bax and vimentin) studies were carried out. Gene expression of *vimentin*, *PCNA*, *CHOP*, *Bcl-2*, *Bax*, and *XBP1* were investigated via quantitative real-time polymerase chain reaction (qRT-PCR), besides estimation of malondialdehyde (MDA) and total antioxidant capacity (TAC). Light and electron microscopic examinations of the testes and epididymis revealed pathological changes emphasizing both mitochondrial injury and ER stress in the AlCl₃ group. Taurine-treated rats showed a noticeable improvement in the testicular and epididymal ultrastructure. Moreover, they exhibited increased gene expression of *vimentin*, *Bcl-2*, and *PNCA* accompanied by decreased *CHOP*, *Bax*, and *XBP1* gene expression. In conclusion, male reproductive impairment is a significant hazard associated with AlCl₃ exposure. Both ER stress and mitochondrial impairment are critical mechanisms of the deterioration in the testes and epididymis induced by AlCl₃, but taurine can amend this.

Keywords Taurine · Testes · ER stress · Mitochondrial injury · PCNA · Vimentin

✉ Fatma E. Hassan
Fatma.e.elsayed@kasralainy.edu.eg

1 Medical Histology and Cell Biology Department, Faculty of Medicine, Mansoura University, Mansoura 35516, Egypt

2 Medical Biochemistry and Molecular Biology Department, Faculty of Medicine, Mansoura University, Mansoura 35516, Egypt

3 Clinical Biochemistry Department, Faculty of Medicine, King Abdulaziz University, Jeddah 21465, Saudi Arabia

4 Medical Physiology Department, Kasr Alainy, Faculty of Medicine, Cairo University, Cairo, Egypt

5 Clinical Pharmacology Department, Faculty of Medicine, Alexandria University, Alexandria, Egypt

Introduction

Aluminum (Al) is an extensively disseminated metal in the environment and can thus potentially cause toxic damage to different human tissues and organs (Shaw 2018). Al compounds are widely used in medicines such as antacids, vaccines, antidiarrheals, phosphate binders, and allergen injections (Igbokwe et al. 2019), food additives, toothpaste (Saad et al. 2018), and water purification agents (Kalaiselvi et al. 2014).

It has been described that aluminum chloride (AlCl₃) produces reactive oxygen species (ROS) (Al-Otaibi et al. 2018) and inhibits antioxidant enzymes in the blood, seminal plasma, testis, liver, kidney, lung, and brain (Güvenç et al. 2020). Excessive production of ROS causes oxidative stress in spermatozoa, producing male infertility (Agarwal and Sengupta 2020). AlCl₃-induced toxicity in the epididymis, vas deferens, seminal vesicle, and ventral prostate of mice

was also reported by ALMurshidi et al. (2021). Moreover, exposure to AlCl$_3$ has been reported to affect testicular development and testosterone synthesis in experimental animals (Lokman et al. 2021).

Xu et al. (2017) found that AlCl$_3$ exposure promotes mitochondrial oxidative stress, which may contribute to mitochondrial energy metabolism disorder and liver dysfunction. Testicular mitochondria regulate different aspects of male reproductive functions, such as spermatogenesis, adenosine triphosphate (ATP) synthesis, and Leydig cell steroidogenesis (Ibrahim et al. 2019). In addition, sperm mitochondria are involved in many essential fertility processes, such as sperm motility, hyperactivation, capacitation, and acrosome reaction (Durairajanayagam et al. 2021).

Furthermore, it was reported that AlCl$_3$ exposure induces endoplasmic reticulum (ER) stress in rat brain (Promyo et al. 2020). Under specific conditions, ER stress can be beneficial to the body; however, if ER protein homeostasis is not restored, the prolonged activation of the unfolded protein response (UPR) may initiate apoptotic cell death via upregulation of the CCAAT enhancer-binding protein (C/EBP) homologous protein (CHOP). CHOP induces apoptosis via suppression of the prosurvival protein B-cell lymphoma-2 (Bcl-2). Bcl-2-associated X (Bax) was also upregulated during ER stress in cardiomyocyte models (Wang et al. 2018). Li et al. (2014) showed that CHOP-deficient mice have less apoptotic cell death and lower caspase-3 activation related to decreased Bax levels.

With the expansion in male reproductive disorders, there is a pressing need to promote male fertility with natural products that are less likely to have negative effects, being more affordable and more compliant. Taurine is an essential β-amino acid that is abundant in most cells, especially excitable tissues (Schaffer and Kim 2018). Taurine has numerous physiological effects, including bile salt production in the liver, membrane stabilization, osmoregulation, neurotransmission modulation, Ca^{2+} homeostasis (Bhat et al. 2020), and mitigation of ER stress through improving protein folding (Ito et al. 2015). Taurine also has antioxidant and energy-producing properties, which help to protect cells (Schaffer et al. 2014; Shetewy et al. 2016). Taurine deficiency is often associated with serious diseases (Schaffer and Kim 2018).

Taurine provides a novel therapeutic option for metabolic illnesses such as diabetes mellitus (Ito et al. 2012), hypercholesterolemia (Sagara et al. 2015), and obesity (Yamori et al. 2010). Taurine has also been reported to improve many other diseases, including hypertension, atherosclerosis, ischemia–reperfusion injury, myocardial arrhythmias, congestive heart failure (Ahmadian et al. 2017; Qaradakhi et al. 2020), skeletal muscular dysfunction (Terrill et al. 2016), cerebral stroke, neurodegenerative diseases (Zhang et al. 2016), epilepsy (Oja and Saransaari 2013), and inflammatory diseases such as arthritis (Marcinkiewicz and

Kontny 2014). In addition, taurine is extremely effective in the treatment of mitochondrial diseases such as mitochondrial encephalopathy (Rikimaru et al. 2012).

However, the roles of ER stress and mitochondrial injury in AlCl$_3$-induced male gonadal damage have not been fully discussed, and the mechanisms of the taurine protective effect against AlCl$_3$-induced male gonadal impairment remain to be studied in full. Therefore, the aim of this study is to investigate the role of ER stress and mitochondrial injury in the pathogenesis of AlCl$_3$-induced testicular and epididymal damage at the histological, biochemical, and molecular levels, in addition to the possible ameliorative effect of taurine.

Materials and methods

Ethical approval statement

All the experimental work was performed following the international guidelines of Helsinki for animal welfare. The study was conducted in the Animal House, Faculty of Medicine, Alexandria University according to the guidelines for the care and use of experimental animals of Alexandria University, approved by the Institutional Animal Care and Use Committee with ethical committee approval IP (IRP no. 00012098-FWA NO:00018699).

Chemicals

Aluminum chloride anhydrous powder (AlCl$_3$, 99.999%, CAS no. 7446-70-0, EC no. 231-208-1, MDL no. MFCD00003422) was obtained from Sigma, Aldrich (St. Louis, MO, USA). To prepare stock solution (20 mg/ml), 2 g AlCl$_3$ was dissolved in 100 ml distilled water. Taurine (Kosher, ≥ 98%) was obtained from Sigma Aldrich (Switzerland, CAS no. 107-35-7, EC no. 203-483-8, MDL no. MFCD 00,008,197) and dissolved in distilled water (62.5 mg/ml at 20 °C), water (65 mg/ml at 12 °C), and dimethylsulfoxide (DMSO) (< 1 mg/ml at 25 °C).

Animals and study protocol

Forty-eight adult male albino Sprague–Dawley rats (90 days old, body weight 230 ± 30 g) were obtained from the Alexandria Experimental Research Center, Alexandria University. Rats were kept in specific pathogen-free conditions, fed normal animal chow, and exposed to a 12:12 h light/ dark regime. Rats were housed in standard cages at a room temperature of 25 ± 2 °C and left to acclimatize for a few days before commencing the experimental procedures. Rats were indiscriminately and equally divided into four groups as follow:

Group I (negative control): rats orally received distilled water 5 ml/kg/day for 8 weeks. Group II (positive control): rats were intraperitoneally (IP) injected with taurine (200 mg/kg, once/day) (Gupte et al. 2019) for 8 weeks. Group III (AlCl$_3$): Rats were orally administered AlCl$_3$ (50 mg/kg/day) by gastric tube (Reichert et al. 2021) for 6 weeks. Group IV (AlCl$_3$ plus taurine): Rats received IP taurine (200 mg/kg, once per day) for 2 weeks followed by a combination of oral AlCl$_3$ (50 mg/kg/day) and IP taurine (200 mg/kg, once/day) for a further 6 weeks.

At the end of the experiment, animals were sacrificed under diethyl ether anesthesia. An abdominal incision was made, and testes and epididymis were carefully dissected. One testis and epididymis from each rat were kept in liquid nitrogen (at −80 °C) for further entire RNA derivation and quantitative real-time polymerase chain reaction (qRT-PCR) analysis of expression of *vimentin*, proliferating cell nuclear antigen (*PCNA*), *CHOP*, *Bcl-2*, *Bax*, and X-box DNA binding protein1 (*XBP1*) as well as estimation of malondialdehyde (MDA) and total antioxidant capacity (TAC). The other testis and epididymis were prepared for histological examination.

Histological study

Specimens from the testis and epididymis were fixed in Bouin's solution, dehydrated in an increasing series of alcohol, cleared in two changes of xylene, and then embedded in molten paraffin. Afterward, sections of 5–6 μm thickness were obtained using a rotary microtome, mounted on clean slides, and stained with hematoxylin and eosin (H&E) (Bancroft and Gamble 2008).

Immunohistochemical (IHC) study of Bax and vimentin proteins

Paraffin sections of testis and epididymis with thickness of 4 μm on positively charged glass slides were immunostained by the avidin–biotin procedure to detect Bax and vimentin proteins. The sections were deparaffinized in xylene and rehydrated in descending grades of alcohol down to distilled water, then treated with 0.3% hydrogen peroxide for 15 min to suppress endogenous peroxidase activity. For antigen retrieval, sections were boiled in citrate buffer (pH 6) for 10 min, then cooled and washed in phosphate-buffered saline (PBS). To diminish nonspecific reactions, sections were incubated with 10% normal goat serum for 30 min, followed by incubation for 1 h with antisera containing primary antibodies. Two primary antibodies were used. The first one was anti-Bax, rat monoclonal antibody (1:50, no. 13401A, clone G206-1276, immunoglobulin [Ig] M, 0.5 mg/mL, PharMingen, San Diego, CA) that was used in rats before according to Khalaf and El-Mansy (2019). The second one was anti-vimentin mouse monoclonal antibody (1:100, clone v9, Dako) that was used in rats before according to Ghoneim et al. (2014). After that, biotinylated secondary antibody (Dako-K0690; Dako Universal LSAB Kit) and streptavidin–biotin peroxidase complex (Dako-K0690) were added for 30 min. The immunoreactivity was visualized using 3,3′-diaminobenzidine (DAB)–hydrogen peroxide as a chromogen (Sigma-D5905; Sigma–Aldrich Company Ltd., Gillingham, UK) for 5 min. Mayer's hematoxylin was used as counterstain. After replacing the primary antibodies with PBS, negative control sections were placed under the same conditions (Figs. 1a–d). The positive control slides for anti-Bax and anti-vimentin were rat thymus and tonsil, respectively (Cemek et al. 2008).

Electron microscopic study

Small pieces (1 mm) of testis and epididymis were fixed in 2.5% glutaraldehyde buffered with 0.1 M sodium cacodylate (pH 7.2) for 2 h and washed three times with the same buffer. After washing, they were post-fixed in phosphate-buffered 1% osmium tetroxide for 2 h at room temperature, then dehydrated in an increasing series of ethanol. After immersion in propylene oxide, sections with thickness of 1 μm were obtained, stained with toluidine blue (1%), and inspected by light microscopy. Sections with thickness of 80–90 nm were cut by using a LKB ultramicrotome then stained with uranyl acetate and lead citrate (Woods and Stirling 2018). Ultrastructural details were inspected by transmission electron microscope (JEOL JEM-2100) (Gatan Inc., Tokyo, Japan) in the Electron Microscopic Unit, Faculty of Agriculture, Mansoura University, Egypt.

Histomorphometrical study

Area percent of Bax and vimentin immunostaining

By image analysis, the area percent of Bax and vimentin immunostaining was measured by examining ten non-overlapping fields from each rat (five rats per group). The slides were photographed with an Olympus digital camera (E24-10 megapixel, China) equipped onto an Olympus microscope through a 0.5× photo-adaptor at magnification of 400×. The resulting images were analyzed on an Intel Core I3-based computer using Video Test Morphology software (Saint Petersburg, Russia) (Sabha et al. 2008).

Epididymal sperm count

The distal cauda of the epididymis was dissected, placed in separate microcentrifuge tubes, minced, and suspended in normal saline at 37 °C for 5 min. A light microscope with a plan objective lens was used to analyze the sperm count (Olympus
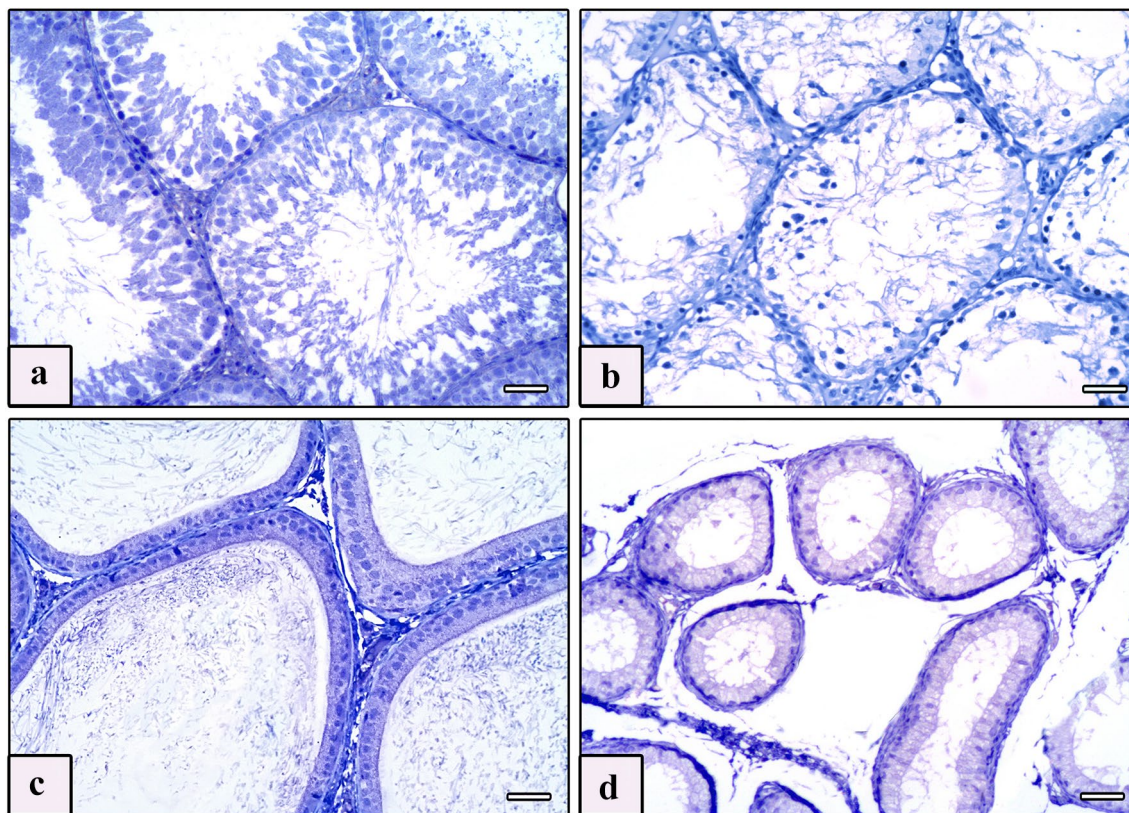
Fig. 1 Photomicrographs of Bax and vimentin negative control sections of testis and epididymis of studied rat groups. **a** Negative control sections of the testis of the control groups. **b** Negative control sections of the testis of the AlCl₃ group. **c** Negative control sections of the epididymis of the control groups. **d** Negative control sections of the epididymis of the AlCl₃ group. Bax and Vimentin, scale bars = 50 μm (**a**–**d**)

CX31 Binocular Microscope. New York Microscope Company, NY, USA). The number of spermatozoa within ten grid squares was counted using a sperm counting chamber (Makler/Sperm Meter, Product Code: Sperm Counting Chamber; SEFI-Medical Instruments, New York, NY, USA). The chamber was prewarmed to 37 °C. Sperm count was expressed as million/ml (Karna et al. 2019a, b).

Leydig cell count

Leydig cells were counted by examining ten non-overlapping sections from each group by an Olympus light microscope with a 0.5× photo-adaptor (OlympusBX40 image analyzer computer system, Cambridge, UK) using a calibrated ocular lens of a micrometer (Germany) to calculate the number per 100 μm² (40× objective lens) (Moustafa et al. 2012; Alasmari et al. 2018).

Biochemical and molecular studies

Measurement of MDA and TAC levels in testicular and epididymal tissues

The testicular and epididymal tissues were perfused with PBS solution, pH 7.4, containing 0.16 mg/ml heparin to remove red blood cells and clots. Then, each tissue sample was homogenized in 5–10 ml cold buffer (50 mM potassium phosphate, pH 7.5, 1 mM EDTA). Homogenates were centrifuged at $10,000 \times g$ for 15 min at 4 °C. The supernatant fluid was separated into aliquots and stored at −80 °C until subsequent assessment of MDA and TAC.

MDA content was measured (in nmol/g tissue) by using the thiobarbituric acid (TBA) reaction as described previously by Draper et al. (1993). The absorbance of samples was measured at 532 nm using a colorimetric kit (cat.

no. MD 2528). TAC was estimated (in ng/mg protein) by using commercially available colorimetric kits (Young 2001) (cat. no. # TA 25 12). Both kits were supplied by Bio-Diagnostics, Dokki, Giza, Egypt.

qRT-PCR of *vimentin*, *Bcl-2*, *Bax*, *PCNA*, *XBP1*, and *CHOP* gene expression in testicular and epididymal tissues

The total RNA was sequestrated from 25–35 mg tissue samples of rat testes and epididymis after snap freezing with liquid nitrogen using Tri-Fast reagent (PeqLab Biotechnologie GmbH, Carl-Thiersch St. 2B 91,052 Erlangen, Germany, cat. no. # 30–2010), triazole, and chloroform according to manufacturer's instructions. Extracted RNA concentration and purity were assessed by Nanodrop 2000 spectrophotometer (Thermo Scientific, USA). Reverse transcription reaction for complementary DNA (cDNA) synthesis was accomplished with ~250 ng total RNA using the Maxima First Strand cDNA synthesis kit (Thermo Scientific, Waltham, MA, USA, cat no. #K1641). Testis and epididymis messenger RNA (mRNA) expression of *vimentin*, *Bcl-2*, *Bax*, *PCNA*, *XBP1*, and *CHOP* were measured by qRT-PCR using the Applied Biosystem 7500 RT-PCR detection system (Life Technology, USA) with HERAPLUS SYBR® Green qPCR Master Mix (2x) (Willowfort, UK, cat. no. WF10308001). The RT-PCR reaction consisted of enzyme activation at 95 °C for 10 min, followed by 40 cycles of two-step cycling, including template denaturation at 95 °C (15 s), then annealing/extension at 60 °C (1 min). The primer sequences utilized were as follow: *vimentin*: forward, 5′-GCA CCC TGC AGT CAT TCA GA-3′; reverse, 5′-GCA AGG ATT CCA CTT TAC GTT CA-3′ (Zhuang et al. 2015); *Bcl-2*: forward, 5′-TGT GGA TGA CTG ACT ACC TGA ACC-3′; reverse, 5′-CAG CCA GGA GAA ATC AAA CAG AGG-3′ (Ghoneim et al. 2020); *Bax*: forward, 5′-GGC GAA TTG GCG ATG AAC TG-3′; reverse, 5′-ATG GTT CTG ATC AGC TCG GG-3′ (AL-Megrin et al. 2020); *PCNA*: forward, 5′- CTG CTG GGA CAT CAG TTC GG-3′; reverse, 5′-GAT CGC AGC GGT ATG TGT CG-3′ (Duan et al. 2020); *XBP1*: forward, 5′- GGT ATA GCC AGC GAG TGC T-3′; reverse, 5′-TCA GTT GGG AGC TG ATT CT-3′ (Zhu et al. 2012); *CHOP*: forward, 5′-GAA AGC AGA AAC CGG TCC AAT-3′; reverse, 5′-GGATGAGATATAGGTGCCCCC-3′ (Idari et al. 2021); *β-actin* (internal control gene): forward, 5′-AAG ATC CTG ACC GAG CGT GG-3′; reverse, 5′-CAG CAC TGT GTT GGC ATA GAG G-3′ (Ghoneim et al. 2020). The expression of the analyzed genes was normalized to that of the internal control gene β-actin using the comparative $\Delta\Delta CT$ method.

Statistical analysis

The obtained data were managed, and analyzed using the Statistical Package for Social Sciences (SPSS) version 15 for Windows (SPSS Inc, Chicago, IL, USA). Quantitative data were first verified for normality by the Kolmogrov–Smirnov test. As the presented data showed a parametric distribution, they are presented as mean $\pm$ standard deviation (SD). The *F* test (one-way analysis of variance test) was applied to compare between more than two groups, followed by Tukey's post hoc test. Differences were considered statistically significant for *P* value < 0.05 (Landau and Everitt 2003).

Results

Light microscopic results

H&E stain

Inspection of testicular tissues of control groups revealed the standard construction of testis structures. Seminiferous tubules (STs) were bounded by a basement membrane with myoid cells. They were lined by stratified spermatogenic cells in addition to Sertoli cells. The spermatogenic cells included spermatogonia, primary spermatocytes, spermatids (rounded and elongated), and spermatozoa. Between STs, the interstitium contained Leydig cells and blood vessels. Leydig cells appeared in clusters or singly, having rounded vesicular nuclei with extensive acidophilic cytoplasm and variable numbers of lipid vacuoles (Fig. 2a).

The $AlCl_3$ group showed apparent distortion in the testicular architecture. STs exhibited many disturbances in the form of degeneration, irregularity, different shapes with wavy outlines, and loss of the normal distribution of the epithelial lining, with the presence of multiple vacuoles between them (Fig. 2b, c). Congested thickened dilated blood vessels, and degenerated spermatogenic cells with multiple large multinucleated cells were noticed (Fig. 2b). Degenerated Leydig cells with darkly stained nuclei and vacuolated or acidophilic cytoplasm were apparent (Fig. 2c). There was a rupture of some tubules. Large multinucleated cells were seen within the lumen of some ruptured tubules with wide interstitial space comprising degenerated Leydig cells with acidophilic cytoplasm (Fig. 2d). Some ruptured tubules exhibited exfoliated pyknotic cells in the lumen, and others showed degenerated spermatogenic cells detached from the basement membrane (Fig. 2e).

Examination of the $AlCl_3$ plus taurine group revealed preserved testicular structure that was almost similar to control groups. The STs were lined by stratified spermatogenic epithelium based on the basement membrane. It contained
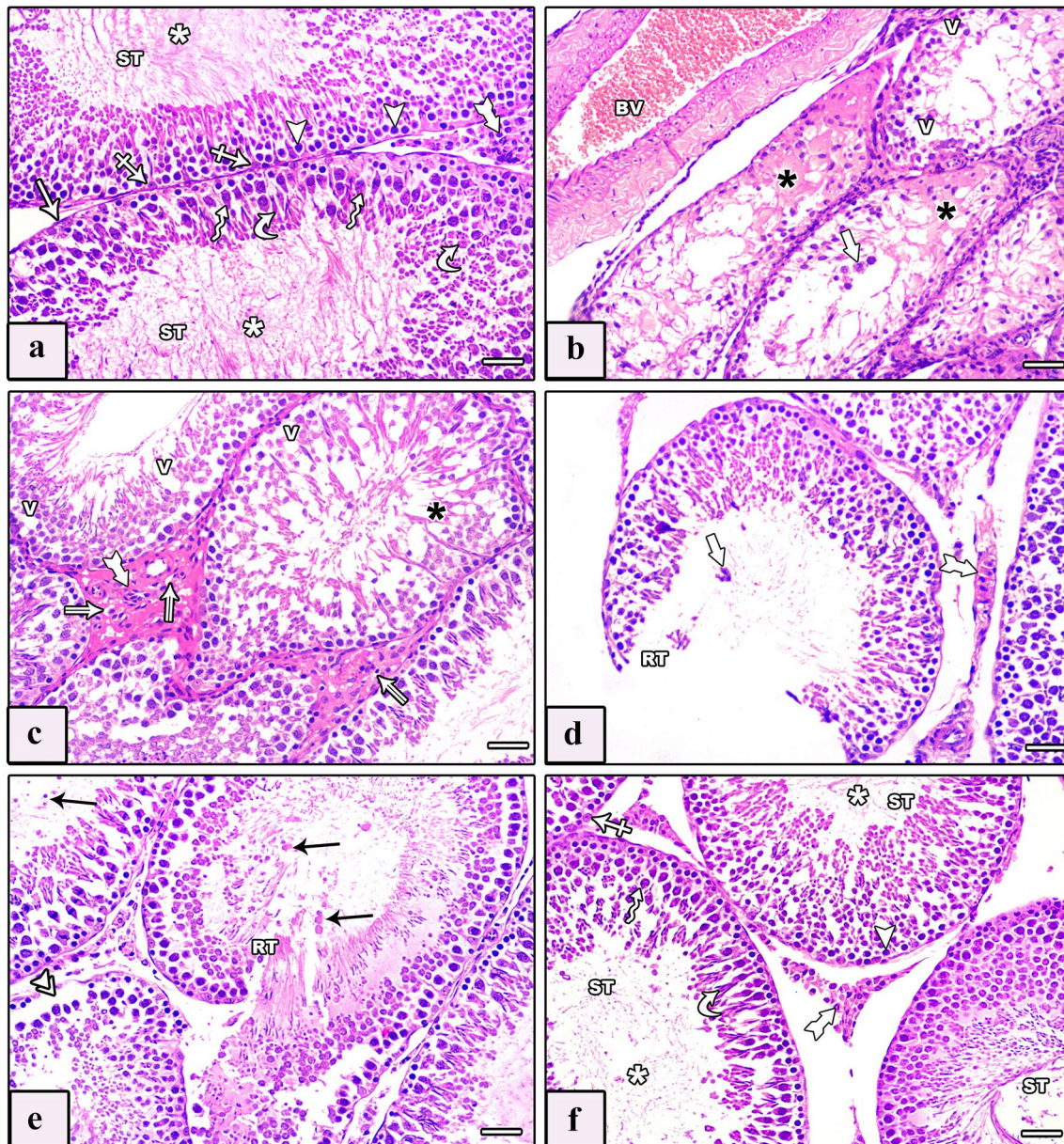
Fig. 2 Photomicrographs of sections of testis of studied rat groups stained with H&E. **a** Control group shows thin regular basement membrane ensheathed by flattened nuclei of myoid cells (arrow). The seminiferous tubule (ST) is lined by spermatogenic cells and Sertoli cells (crossed arrows). Spermatogenic cells include spermatogonia (arrowheads), primary spermatocytes (zigzag arrows) and spermatids (curved arrows) with intraluminal spermatozoa (white asterisk). The tubules are separated by interstitial tissue showing Leydig cells (tailed arrow). **b–e** AlCl₃ group shows a disorganized testicular architecture. **b** Congested thickened dilated blood vessel (BV) is seen. Seminiferous tubules exhibit degeneration and irregularity with loss of their lining (black asterisk), multiple vacuoles (V) between spermatogenic cells, and large multinucleated cells (thick arrow) within the lumen of some tubules. **c** Different shapes and wavy outlines of seminiferous tubules with loss of their epithelial lining (black asterisk) and multiple vacuoles (V) between them are seen. Degenerated Leydig cells with darkly stained nuclei and vacuolated (double arrow) or acidophilic (tailed arrow) cytoplasm are seen. **d** Ruptured tubules (RT) with large multinucleated cells (thick arrow) within their lumen and wide interstitial space containing degenerated Leydig cells with acidophilic cytoplasm (tailed arrow) are seen. **e** Ruptured tubules (RT) are seen with exfoliated pyknotic cells in the lumen (arrows), others show degenerated detached spermatogenic cells from the basement membrane (double arrowhead). **f** AlCl₃ plus taurine group shows normal lining of seminiferous tubules (ST), spermatogonia (arrowhead), primary spermatocyte (zigzag arrow), spermatid (curved arrow), and Sertoli cells (crossed arrow). Note the presence of spermatozoa in their lumens (white asterisk) and less wide interstitial tissue containing normal Leydig cells (tailed arrow). H&E, scale bars = 50 μm (**a–f**)

spermatozoa in the lumen and was disconnected by a less wide interstitial tissue containing Leydig cells. Leydig cells appeared with rounded vesicular nuclei and extensive acidophilic cytoplasm (Fig. 2f).

The epididymis of the control groups exhibited regular spherical tubules lined by pseudostratified columnar epithelium with stereocilia based on a thin basement membrane that was surrounded by thin layers of circular smooth muscle. The epithelium showed three types of cells: principal, basal, and apical. A plug of sperm was seen in the tubular lumen. The extratubular interstitium contained blood vessels (Fig. 3a). Epididymis of the AlCl$_3$ group revealed fewer spermatozoa in the lumen of some tubules, while others were empty. Its lining was irregular, stratified, and surrounded by a thick layer of smooth muscle fibers with vacuolated cytoplasm and many exfoliated cells inside the lumen. Wide interstitium contained congested dilated blood vessels,

and mononuclear cellular infiltration was seen (Figs. 3b , c). In the AlCl$_3$ plus taurine group, the epididymis was almost identical to that of the control group, exhibiting regular spherical tubules lined by pseudostratified columnar ciliated epithelium based on a thin basement membrane encircled by thin layers of circular smooth muscles (Fig. 3d).

Immunohistochemical stains

Anti-Bax

Examination of Bax immunostained sections of the testis of control groups displayed negative cytoplasmic immunoreaction in the interstitial cells of Leydig (Fig. 4a), whereas immunostained sections from the AlCl$_3$ group showed intensive immunoreaction (Fig. 4b, c). In the immunostained sections of the AlCl$_3$ plus taurine group, the immunoreaction in
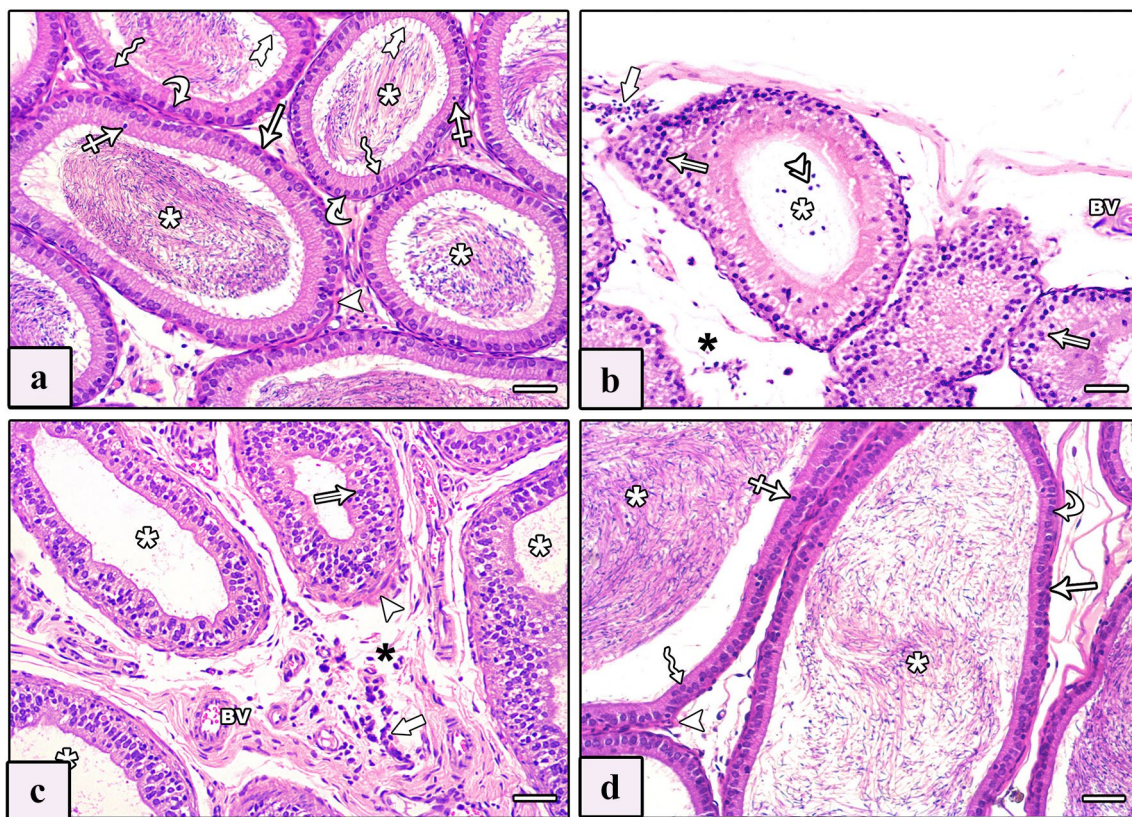

Fig. 3 Photomicrographs of sections of epididymis of studied rat groups stained with H&E. **a** Control group: the epididymis exhibits regular spherical tubules lined by pseudostratified columnar epithelium with stereocilia (tailed arrows) based on a thin basement membrane (arrow) and surrounded by thin layers of circular smooth muscle (arrowhead). The epithelium shows three types of cells: principal (zigzag arrows), basal (curved arrow), and apical (crossed arrows). A plug of sperm is seen in the tubular lumen (asterisk). **b**, **c** AlCl$_3$ group: epididymal lining is irregular, stratified with vacuolated cytoplasm (double arrows) and surrounded by a thick layer of smooth muscle fibers (arrowhead). There are many exfoliated cells inside

the lumen (double arrowhead), reduced spermatozoa in the lumen of some tubules with the presence of empty ones (white asterisk), and wide interstitium (black asterisk) containing congested dilated blood vessel (BV) and mononuclear cellular infiltration (thick arrow). **d** AlCl$_3$ plus taurine group: the epididymis shows normal epithelial lining of tubules, with principal (zigzag arrows), basal (curved arrow), and apical (crossed arrows) cells based on a thin basement membrane (arrow) surrounded by thin layers of circular smooth muscle (arrowhead). A plug of sperm (white asterisk) is seen in the lumen of tubules. H&E, scale bars = 50 μm (**a–d**)
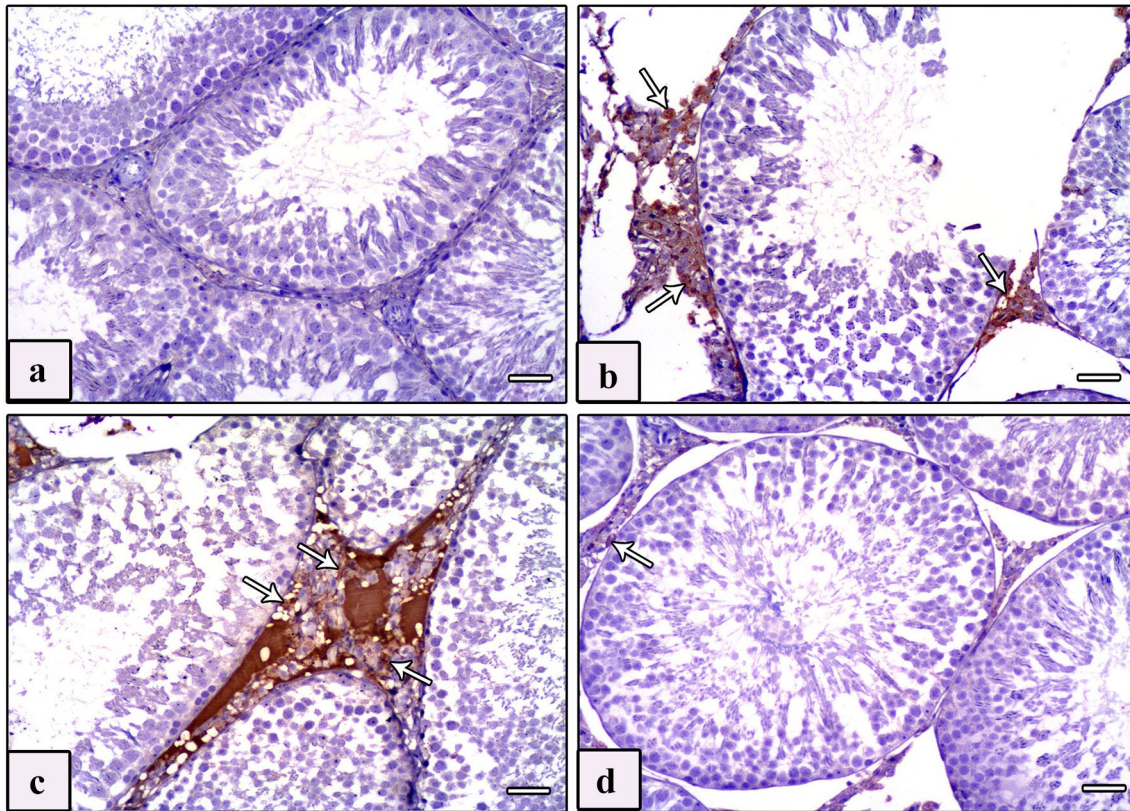
Fig. 4 Photomicrographs of sections of testis of studied rat groups stained with Bax immunostaining. **a** Control group shows negative immunoreaction in the cytoplasm of the interstitial cell of Leydig. **b**, **c** AlCl₃ group reveals intensive immunoreaction in the cytoplasm of interstitial cells of Leydig (arrows). **d** AlCl₃ plus taurine group shows minimal immunoreaction in the cytoplasm of interstitial cells of Leydig (arrows). Bax, scale bars = 50 µm (**a**–**d**)

the cytoplasm of the interstitial cells of Leydig was negligible (Fig. 4d). Examination of Bax immunostained sections of the epididymis revealed negative immunoreaction in the epididymal cell lining of control groups (Fig. 5a). Intensive immunoreaction in almost the whole epididymal cell lining of the AlCl₃ group was noticed (Fig. 5b). In the AlCl₃ plus taurine group, the immunoreaction in the epididymal cell lining was minimal (Fig. 5c).

Anti-vimentin

Examination of vimentin-immunostained sections of testis of control groups revealed typical flame-like vimentin immunoreaction of Sertoli cells. The reaction was located in the perinuclear regions and midportions, and increasingly reached the apex of the cytoplasm. A robust positive immune reaction was detected in the cytoplasm of Leydig cells, endothelial cells of blood vessels, and smooth muscle cells (Fig. 6a). However, vimentin-immunostained sections of testes of the AlCl₃ group revealed a positive immunoreaction limited to the perinuclear region of Sertoli cells with loss of the typical flame-like appearance as well as a positive immunoreaction in the interstitial Leydig cells and a moderate reaction in the blood vessels (Fig. 6b, c). Meanwhile, vimentin-immunostained sections of testes of the AlCl₃ plus taurine group revealed a flame-like positive cytoplasmic immunoreaction spreading to the apical parts of the majority of Sertoli cells. Moreover, a positive immune reaction was detected in the Leydig cells and blood vessels (Fig. 6d). Examination of vimentin-immunostained sections of the epididymis of control groups revealed strong immune reaction in the peritubular myoid cells, the smooth muscle layer, and the cytoplasm of endothelial cells of blood vessels in the interstitial tissue between the epididymal ducts (Fig. 7a). However, vimentin-immunostained sections of the epididymis of the AlCl₃ group revealed a faint immune reaction in the peritubular myoid cells, thickened smooth muscle layer, and cytoplasm of endothelial cells (Fig. 7b). Vimentin-immunostained sections of the epididymis of the AlCl₃ plus taurine group exhibited restoration of the standard immune reaction as in control groups (Fig. 7c).
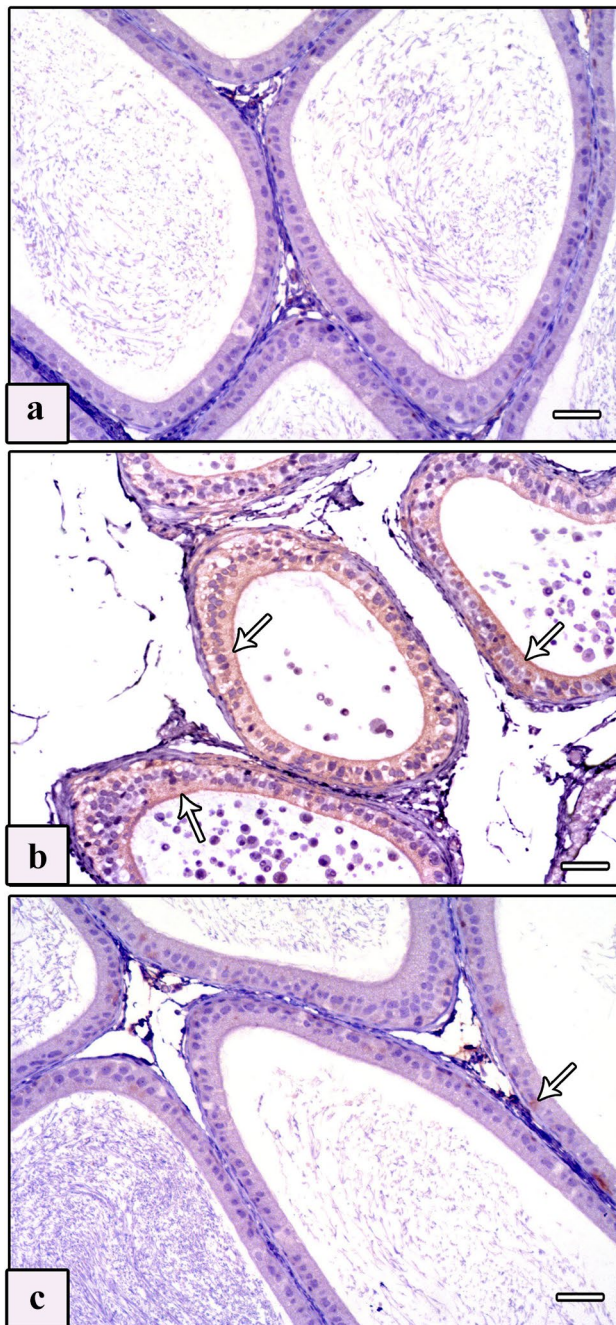
Fig. 5 Photomicrographs of sections of epididymis of studied rat groups with Bax immunostaining. **a** Control group shows negative immunoreaction in the epididymal cell lining. **b** AlCl$_3$ group reveals intensive immunoreaction in approximately all epididymal cell lining (arrows). **c** AlCl$_3$ plus taurine group shows minimal immunoreaction in the epididymal cell lining (arrows). Bax, scale bars = 50 μm (**a–c**)

Electron microscopic results

Electron microscopic (EM) investigation of the ultrathin sections of the testes of control groups showed Sertoli cells lying on a regular thin basement membrane with myoid cells.

They were huge oval cells that had large indented euchromatic nucleus with a prominent nucleolus. Their cytoplasm exhibited mitochondria, rough ER (rER), and ribosomes, besides lysosomes (Fig. 8a). The AlCl$_3$ group showed an apparent increase in the number of distorted Sertoli cells resting on thickened irregular basement membrane with myoid cells. Irregular heterochromatic nuclei of Sertoli cells with ring-shaped and vacuolated mitochondria, swollen rER, many lysosomes, and cytoplasmic vacuolations were seen (Fig. 8b–d). The AlCl$_3$ plus taurine group displayed Sertoli cell resting on normal basement membrane with maintained ultrastructural picture despite the presence of some vacuolated mitochondria (Fig. 8e).

Spermatogonia of the control groups exhibited oval euchromatic nuclei with prominent nucleolus and peripheral heterochromatin clumps, and its cytoplasm contained mitochondria with characteristic cristae (Fig. 9a). The AlCl$_3$ group showed distorted spermatogonia with heterochromatic nuclei and dilated perinuclear spaces. Their cytoplasm showed degenerated mitochondria and dilated swollen rER (Fig. 9b). The AlCl$_3$ plus taurine group displayed spermatogonia with preserved ultrastructural picture apart from the presence of some vacuolated mitochondria (Fig. 9c).

The ultrastructure of primary spermatocytes of the control groups showed cells with rounded euchromatic nuclei displaying synaptonemal complexes. Their cytoplasm revealed peripherally arranged mitochondria (Fig. 10a). The AlCl$_3$ group showed primary spermatocytes with shrunken heterochromatic nuclei. Their cytoplasm revealed vacuolated mitochondria besides dilated and swollen rER (Fig. 10b). The AlCl$_3$ plus taurine group demonstrated conservation of the normal ultrastructural appearance of primary spermatocytes despite the presence of some vacuolated mitochondria (Fig. 10c).

EM examination of ultrathin sections of the early spermatids of the control groups showed rounded spermatids with spherical euchromatic nuclei. They had regular acrosomal caps covering the anterior parts of the nuclei, linked with dense acrosomal granules. Their cytoplasm revealed a well-formed obvious Golgi and peripheral mitochondria (Fig. 11a). In the AlCl$_3$ group, the spermatids had degenerated. Some cells had shrunken heterochromatic nuclei, and others showed euchromatic nuclei and ill-developed acrosomal caps. The cytoplasm showed degenerated, vacuolated, and ring-shaped mitochondria in addition to dilated and swollen rER (Figs. 11b, c). The AlCl$_3$ plus taurine group demonstrated a comparatively normal ultrastructural picture despite the presence of vacuolated cytoplasm (Fig. 11d).

The ultrastructure of spermatozoa of the control groups displayed their distinctive appearance; the heads exhibited an elongated electron-dense nuclei, while transverse sections of the tails exhibited middle, principal, and end pieces (Fig. 12a). Each middle piece comprised (from inside to
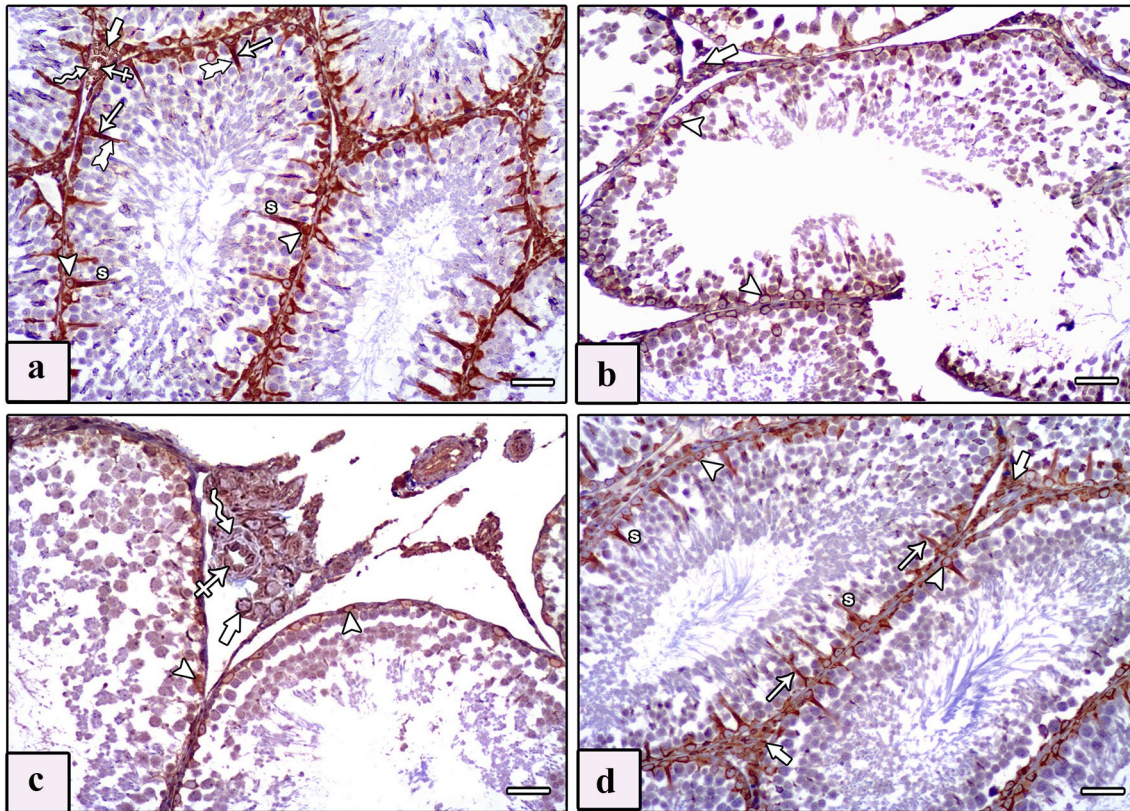
Fig. 6 Photomicrographs of sections of testis of studied rat groups stained with vimentin immunostaining. **a** Control group shows a strong brown, positive immune reaction in the cytoplasm of Sertoli cells (S) with characteristic flame-like vimentin immune reaction located in the perinuclear regions (arrowhead), midportions (arrow), and apices (tailed arrow) of their cytoplasm. Intensive positive immune reaction is seen in the cytoplasm of Leydig cells (thick arrow), the cytoplasm of endothelial cells of the blood vessel (crossed arrow), and in the smooth muscle cells (zigzag arrow). **b**, **c** Vimentin-immunostained sections of testes of $AlCl_3$ group reveal a positive immunoreaction limited to the perinuclear region of Sertoli cells (arrowhead) with loss of the typical flame-like appearance as well as a positive immune reaction in the interstitial Leydig cells (thick arrow), a moderate reaction in the endothelial cells of blood vessels (crossed arrow), and a faint reaction in smooth muscle layer (zigzag arrow). **d** Vimentin-immunostained sections of testes of $AlCl_3$ plus taurine group reveal a flame-like positive cytoplasmic immunoreaction spreading from the perinuclear region (arrowhead) to the apical parts (arrows) of the majority of Sertoli cells (S). Also, a positive immune reaction is seen in Leydig cells (thick arrows). Vimentin, scale bars = 50 μm (**a**–**d**)

out) central axoneme, nine outer dense fibers, mitochondrial sheath, and plasma membrane. Principal piece was composed of a central axoneme, nine dense outer fibers, two longitudinal columns (ventral and dorsal) connected by transverse circumferential ribs, and a plasma membrane. The end piece comprised a central axoneme and plasma membrane (Fig. 12b). The $AlCl_3$ group showed spermatozoa having degenerated heads and many vacuolations in their retained cytoplasm. The middle pieces of their tails showed abnormal outlines with incomplete mitochondrial sheaths (Fig. 12c). The $AlCl_3$ plus taurine group exhibited a normal ultrastructural picture of the spermatozoa regarding their heads and tails (Fig. 12d).

The ultrastructure of Leydig cells of the control groups showed normal structural details with oval euchromatic nuclei, cytoplasm revealed mitochondria, smooth ER (sER), and rER (Fig. 13a). The $AlCl_3$ group showed degenerated

Leydig cells. Some cells appeared with euchromatic nuclei, and others with shrunken heterochromatic nuclei. The cytoplasm revealed dilated and swollen both sER and rER, besides degenerated and vacuolated mitochondria (Fig. 13b, c). The $AlCl_3$ plus taurine group displayed Leydig cells with a well-preserved ultrastructural picture despite some vacuolated mitochondria and dilated sER in their cytoplasm (Fig. 13d).

Histomorphometrical results

Regarding the area percent of Bax immunoreaction of testis (Fig. 14a) and epididymis (Fig. 15a), a statistically significant increase in the $AlCl_3$ group and a non-significant difference in the $AlCl_3$ plus taurine group were observed in comparison with control groups. A significant decrease in the area percent of vimentin immunoreaction of both testes
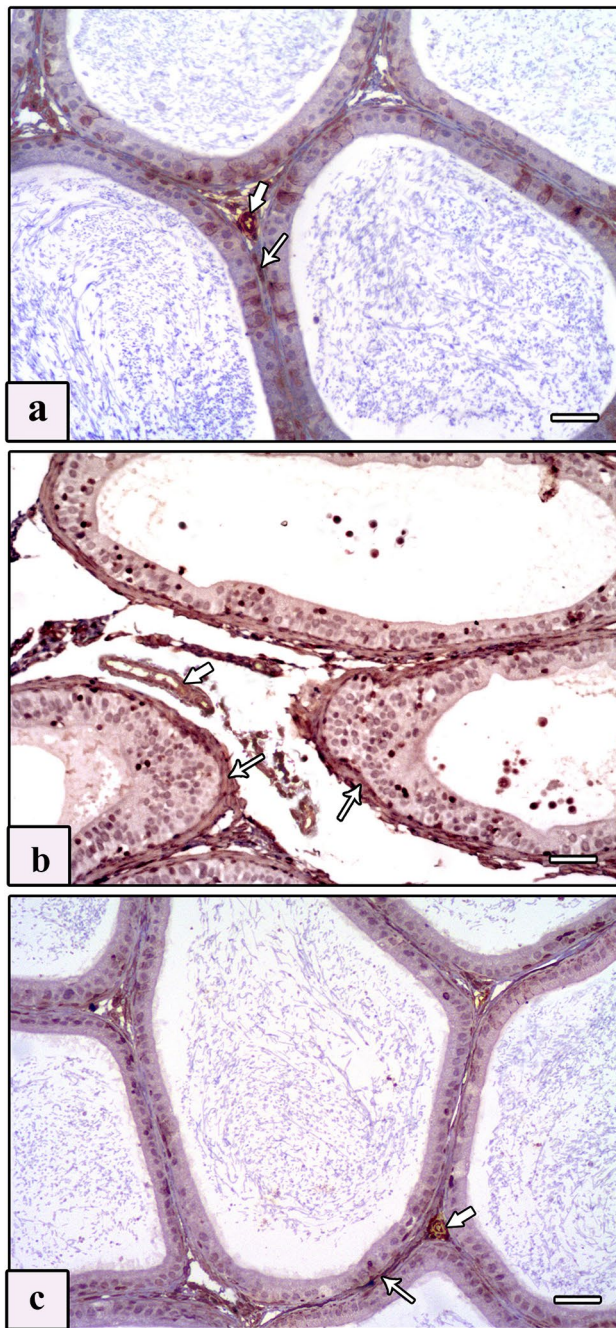
Fig. 7 Photomicrographs of sections of epididymis of studied rat groups stained with vimentin immunostaining. **a** Control group shows a strong immune reaction in the peritubular myoid cells (arrow), smooth muscle layer (curved arrow), and cytoplasm of endothelial cells of blood vessels (thick arrow) present in the interstitial tissue between the epididymal ducts. **b** AlCl₃ group shows a faint immune reaction in the peritubular myoid cells (arrow), thickened smooth muscle layer (curved arrow), and cytoplasm of endothelial cells (thick arrow) **c** AlCl₃ plus taurine group reveals a strong immune reaction in the peritubular myoid cells (arrow), smooth muscle layer (curved arrow), and cytoplasm of endothelial cells (thick arrow). Vimentin, scale bars = 50 μm (**a–c**)

(Fig. 14b) and epididymis (Fig. 15b) in the AlCl₃ group and a non-significant variation in the AlCl₃ plus taurine group were observed in comparison with control groups. A statistically significant reduction in Leydig cell count (Fig. 14c) and epididymal sperm count (Fig. 15c) in the AlCl₃ group and a nonsignificant alteration in the AlCl₃ plus taurine group relative to control groups were detected.

Biochemical results

The results of the current study revealed a significant increase in MDA (lipid peroxidation marker) and a significant decrease in TAC in both the testicular (Figs. 14d, 15d) and epididymal (Figs. 14e, 15e) tissues of AlCl₃ rats compared with control groups. In the AlCl₃ plus taurine group, MDA was significantly lower than in the AlCl₃ group but still higher than that of the control groups, in both tissues. Meanwhile, TAC displayed a significant increase relative to the AlCl₃ group with non-significant changes compared with control groups.

Molecular results

In the current study, apoptosis was confirmed at the molecular level by increased *Bax* (Figs. 14g, 15g) and decreased *Bcl-2* (Figs. 14h, 15h) gene expression in AlCl₃ versus control rats. At the molecular level, decreased *vimentin* expression (Figs. 14f, 15f) was noticed in support of the faint immunoreaction reported at the immunohistochemical level. In addition, a decrease in the cell proliferation factor (*PCNA*) gene expression (Figs. 14i, 15i) was detected in AlCl₃ compared with control rats. ER stress markers were analyzed at the molecular level by measuring the gene expression of *XBP1* (Figs. 14j, 15j) and *CHOP* (Figs. 14k, 15k), revealing a significant increase in AlCl₃ compared with control rats.

In the AlCl₃ plus taurine rats, there was a significant change in the gene expression of the measured parameters compared with the AlCl₃ group in the form of decreased *CHOP*, *Bax*, and *XBP1* but increased *Bcl-2*, *vimentin*, and *PCNA* gene expression. These results confirm the protective effect of taurine against AlCl₃-induced male gonadal damage that was detected above at the histological and biochemical levels.

Discussion

The current study evaluated the harmful effects of AlCl₃ on the testes and epididymis in rats. Administration of AlCl₃ to male rats at a dosage of 50 mg/kg/day for 6 weeks led to oxidative stress, reflected as increased testicular and epididymal MDA. These results follow the findings of El-gayar (2016),
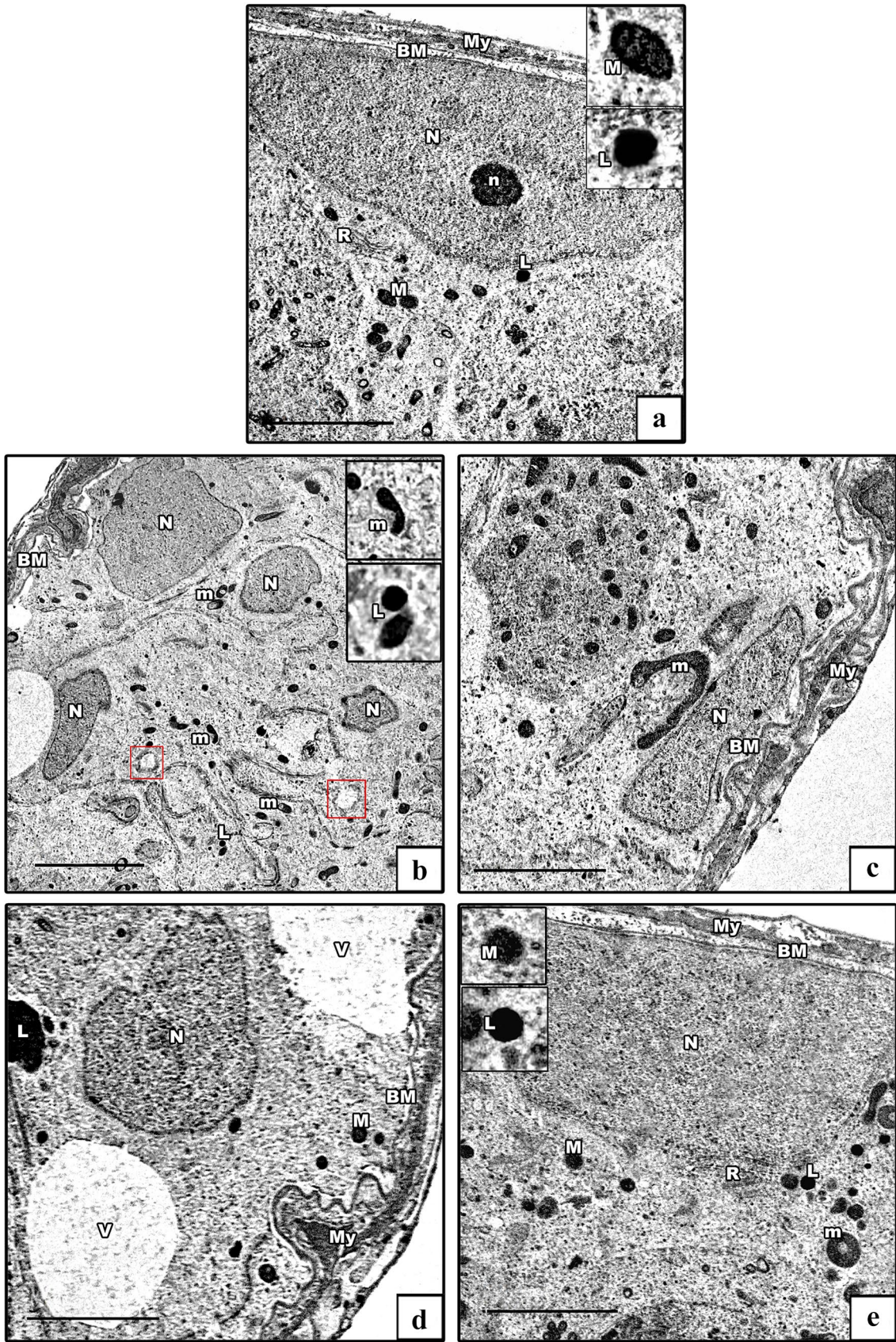
◀**Fig. 8** Electron micrographs of Sertoli cells. **a** Control group shows Sertoli cell resting on a regular basement membrane (BM) with myoid cell (My). It has a large oval euchromatic nucleus (N) with a prominent nucleolus (n). Its cytoplasm shows mitochondria (M), rER (R), and lysosomes (L). The insets show normal mitochondria with preserved cristae and lysosomes. **b–d** AlCl₃ group shows distorted Sertoli cells resting on thickened irregular basement membrane (BM) containing myoid cells (My). They have irregular heterochromatic nuclei (N), ring-shaped and vacuolated mitochondria (m), swollen rER (red box), lysosomes (L), and vacuolated cytoplasm (V). The insets in b show degenerated ring-shaped mitochondria and lysosomes. **e** AlCl₃ plus taurine group: normal Sertoli cell resting on a thin regular basement membrane (BM) with myoid cell (My). It has an oval nucleus (N), normal mitochondrion (M), normal rER (R), and lysosomes (L). The insets show normal mitochondrion with preserved cristae and lysosomes. Notice the presence of some vacuolated mitochondria. Transmission electron microscope, scale bars=5 μm (**a**, **c**, **d**, **e**), 10 μm (**b**)

Yang et al. (2019), and Xu et al. (2020). Lipid peroxidation is the fundamental driver of testicular distortion and consequent dysfunction. Testicular tissue is highly vulnerable to the hazardous effect of free radicals and oxidative stress. This is attributable to numerous explanations involving hyperactive meiosis, cell competition for oxygen rate, low oxygen pressure because of weakened vessels, elevated concentrations of unsaturated fatty acids, and incapability to counteract all free radicals (Asadi et al. 2017), which was confirmed in our study by the suppressed gonadal antioxidants represented by decreased TAC.

Exposure to AlCl₃ led to significant distortion of the testicular architecture, as previously reported by Pandey and Jain (2013) and Nuhair (2015) in AlCl₃-exposed animals and confirmed by Khafaga (2017) and Akinola et al. (2021). Guo et al. (2006) and Berihu (2015) stated that these changes were due to excessive Al deposition in rat sera, testis, and epididymis.

In our study, the imbalance between oxidants and antioxidants was associated with an upregulation of the proapoptotic *Bax* and downregulation of the antiapoptotic *Bcl-2*. This was evident by increased expression and immunoreactivity of *Bax* concomitant with decreased expression of *Bcl-2* in both testicular and epididymal tissues in the AlCl₃ group. This imbalance could explain the histological and apoptotic changes observed at the light microscope level in our study. This aligns with the findings of Ahmed and Mohammed (2021).

Moreover, in the AlCl₃ group, the degenerated spermatogenic cells detached from the basement membrane of STs and the appearance of Sertoli cells resting on thickened irregular basement membrane with myoid cells could be explained by the defective *vimentin* expression and immunoreactivity as also revealed in our study. This could be a result of AlCl₃-induced oxidative stress. Vimentin is typically expressed in the basal and perinuclear regions of Sertoli cells and then radiates toward the apical cytoplasm, associated with desmosome-like junctions between the Sertoli cells and adjacent germ cells. Vimentin plays a role in anchoring germ cells to seminiferous epithelium and maintaining the process of proper spermatogenesis through their dissemination in the Sertoli cells via augmenting the contractions of the STs with subsequent transport of spermatozoa and testicular fluid (Nguyen et al. 2019). Diminished *vimentin* expression and immunoreactivity mirror the associated damage of vimentin filaments, leading to the disintegration of the seminiferous epithelium with subsequent defective spermatogenesis (Fang et al. 2017). Thus, the defective spermatogenesis observed in our study could be due to either the decreased expression of *vimentin* and/or the direct impact of oxidative stress on spermatogenesis or testicular tissues (Alam and Kurohmaru 2014; Heinrich et al. 2020).

AlCl₃-induced oxidative stress and the accompanying prominent apoptosis could inhibit the proliferation and differentiation of Leydig and Sertoli cells, with a subsequent decrease in sperm density and structural damage of the testes and epididymis (Barati et al. 2020). Our results showed a significant decrease of the Leydig cell count in the AlCl₃ group compared with the controls, as reported previously by Nna et al. (2017). Moreover, the significant low gene expression of testicular *PCNA* could explain the AlCl₃-induced spermatogenesis dysfunction in the testis and the lower epididymal sperm count. It has been reported that PCNA is a cell proliferation factor that plays a central role in spermatogenic differentiation and hence spermatogenesis (Panahi et al. 2020).

Furthermore, AlCl₃-associated mitochondrial damage was a prominent feature in the present study in Sertoli and Leydig cells, rounded spermatids, primary spermatocytes, spermatogonia, and spermatozoa. These findings were in agreement with those of Arab-Nozari et al. (2019) and Skalny et al. (2021).

Mitochondrial damage could result from disruption and collapse of the mitochondrial membrane caused by peroxidation of mitochondrial membrane lipids (Koppers et al. 2008) and oxidation of thiol groups of membrane proteins by the increased ROS (Dera and Abushouk 2015). It has also been reported that AlCl₃ alters the mitochondrial oxidative phosphorylation and electron transfer chain activity, with consequent increased oxidative stress (Iglesias-González et al. 2017), as observed in our study.

Bcl-2 is located in the outer mitochondrial membrane and is essential for regulation of mitochondrial membrane permeability and energy metabolism (Giménez-Cassina and Danial 2015). Another mechanism is the AlCl₃-induced disturbed mitochondrial transmembrane potential and opening of mitochondrial permeability transition pores (Liu et al. 2020). This leads to uncontrolled entry of water and solutes into the mitochondria, with consequent mitochondrial swelling and damage upon decreased antiapoptotic protein *Bcl-2*

Fig. 9 Electron micrographs of spermatogonia. **a** Control group ▶ shows a spermatogenic cell with an oval euchromatic nucleus (N) with a prominent nucleolus (n). Its cytoplasm shows mitochondria (M) with characteristic cristae and rER (R). **b** AlCl$_3$ group shows distorted spermatogenic cell. It has a heterochromatic nucleus (N) with a wide perinuclear space (arrow), vacuolated mitochondrion (m), dilated rER (r), and swollen rER (red box). **c** AlCl$_3$ plus taurine group: normal spermatogenic cell with an oval euchromatic nucleus (N), normal mitochondria (M), and normal rER (R). Note the presence of some vacuolated mitochondria (m). Transmission electron microscope, scale bars = 5 μm (**a–c**)

expression (Bonora et al. 2020), as observed in our study. Moreover, Bcl-2 can hinder Bax activation. Bax is a cytosolic protein that could be changed, incorporated into the exterior mitochondrial membrane, and oligomerized. These oligomers might enhance the mitochondrial membrane permeability (Giacomello et al. 2020), resulting in cytochrome *c* release that triggers caspase stimulation and apoptosis (Ibrahim et al. 2019). Thus, the elevated Bax/Bcl-2 ratio is a biomarker of mitochondrial dysfunction (Chiu et al. 2018).

Dysregulation of mitochondrial activity is associated with excessive ROS formation, reduced mitochondrial membrane potential, and ROS-mediated activation of apoptosis signal-regulating kinase 1 (ASK1)/p38 mitogen-activated protein kinase (p38MAPK) (Cheng et al. 2017). So, AlCl$_3$ could cause excessive ROS production and oxidative stress induction, which eventually triggers mitochondrial-mediated apoptosis, playing an essential role in the pathogenesis of AlCl$_3$-induced male gonadal disorders (Lu et al. 2020; Dutta et al. 2021).

Distorted and dysfunctional spermatozoa mitochondrial morphology with subsequent peroxidative destruction of the midpiece and sperm membrane lipids on exposure to AlCl$_3$ contribute to gonadal disorders with diminished fertilization ability of spermatozoa (Jurkowska et al. 2019), as seen in the present study. Besides structural sperm proteins, proteins secreted by the epididymis and cytoplasmic repair enzymes are also damaged by ROS (Chianese and Pierantoni 2021).

Similarly, ER stress was profound in this study following exposure to AlCl$_3$, as seen on EM examination with concomitant increased *XBP1* and *CHOP* gene expression in both testicular and epididymal tissues. This is in agreement with the findings of Okail et al. (2020) in the reproductive tract, Al-Kahtani (2010) in the renal convoluted tubular cells, Abdel-Moneim (2013) in the testis, Alghamdi (2018) in the prefrontal cortex, and Aboelwafa et al. (2020) in the hippocampus.

This abnormal ER morphology with consequent ER dysfunction could be explained by the AlCl$_3$-induced cellular oxidative stress triggering accumulation of unfolded proteins in ER, resulting in its dilatation and swelling (Promyo et al. 2020). However, it might be due to a direct effect of oxidative stress-induced ER membrane damage (Skalny et al.
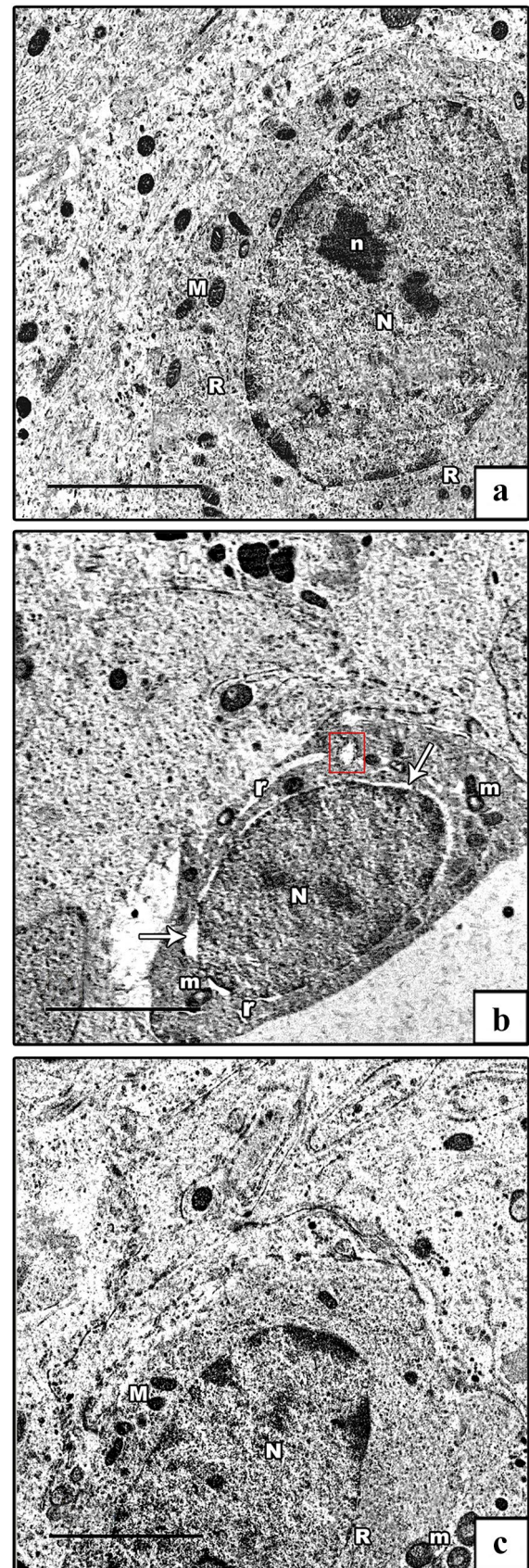
Fig. 10 Electron micrographs of primary spermatocyte. **a** Control ▶ group demonstrates a primary spermatocyte with an oval euchromatic nucleus (N) showing synaptonemal complex (arrow). Its cytoplasm shows rER (R) and peripherally arranged mitochondria (M). **b** AlCl₃ group shows distorted primary spermatocyte. It has a heterochromatic shrunken nucleus (n), swollen rER (red box), and vacuolated mitochondria (m). **c** AlCl₃ plus taurine group: normal primary spermatocyte with an oval euchromatic nucleus (N), normal rER (R), normal mitochondria (M), and vacuolated one (m). Transmission electron microscope, scale bars = 5 μm (**a–c**)
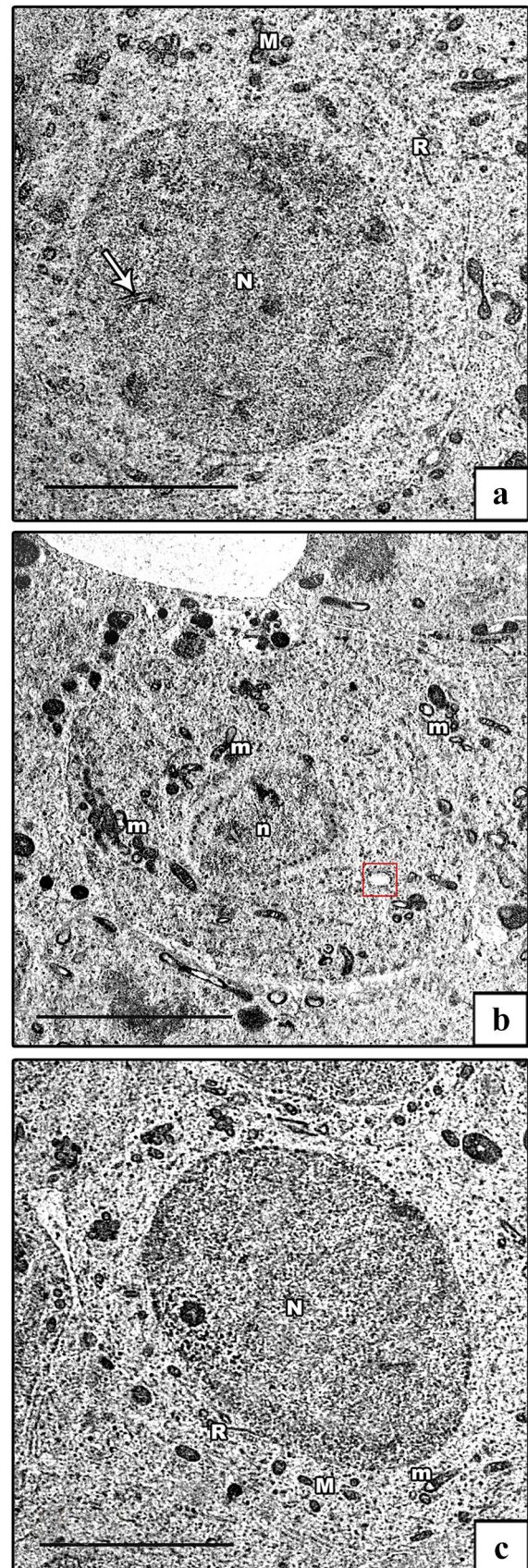
2021) with subsequent activation of an ER-associated protein degradation pathway (ERAD). ERAD is a direct activator of the ER-mediated apoptosis process via downregulation of *Bcl-2* and depletion of cellular antioxidants (Sano and Reed 2013), as presented in our study. Specific inducers mediate ER stress apoptosis, the CHOP transcription factor, and the proapoptotic factor Bax, causing a deficiency of the cellular antioxidant capacity, more oxidative stress, and enhancement of apoptosis, as observed in the current study.

Huo et al. (2004) stated that ER chaperone 78-kDa glucose-regulated protein (Grp 78) is present in spermatocytes, so the ER stress signaling pathway is involved in spermatogenesis and as a signaling mechanism for germ cell apoptosis through stimulation of transcription factor 6 (ATF6), inositol requiring enzyme 1 (IRE1), and protein kinase RNA-activated-like ER kinase (PERK). The activation of PERK and IRE1 pathways principally initiates apoptosis under persistent ER stress. Under ER stress, BiP/Grp78 is titrated away by misfolded proteins, leaving p38MAPK primarily activated by stress-related stimuli. It is mainly associated with germ cell apoptosis. Thus, ER stress plays a role in male gonadal function, posttesticular sperm maturation in the epididymis, and fertility capacity (Karna et al. 2019a, b).

In response to ER stress, IRE1α autophosphorylation activates the expression of an active form of XBP1 with potent transcriptional activity. The active XBP1 provokes expression of UPR/ER stress target genes, which induces the inflammatory cytokine's genes by enhancing Toll-like receptor signaling and promoting differentiation of B lymphocytes and inflammatory response (Kim et al. 2015). In the current study, *XBP1* gene expression increased in the AlCl₃ group, confirming ER stress in testis and epididymis. Hosseini et al. (2020) reported increased *XBP1* expression in the testis and accessory male gonads in response to varicocele-induced oxidative stress and concomitant ER stress, which was confirmed by our results.

The potential protective and therapeutic efficacy of taurine against AlCl₃-induced deleterious effects was previously reported by Abdel-Moneim (2013), Saad et al. (2018), Wenting et al. (2014), and Niu et al. (2018) on testes, kidney, brain, and memory impairment, respectively. In the current study, we attempted to explore the possible protective effects and the underlying mechanisms of taurine on testes and epididymis
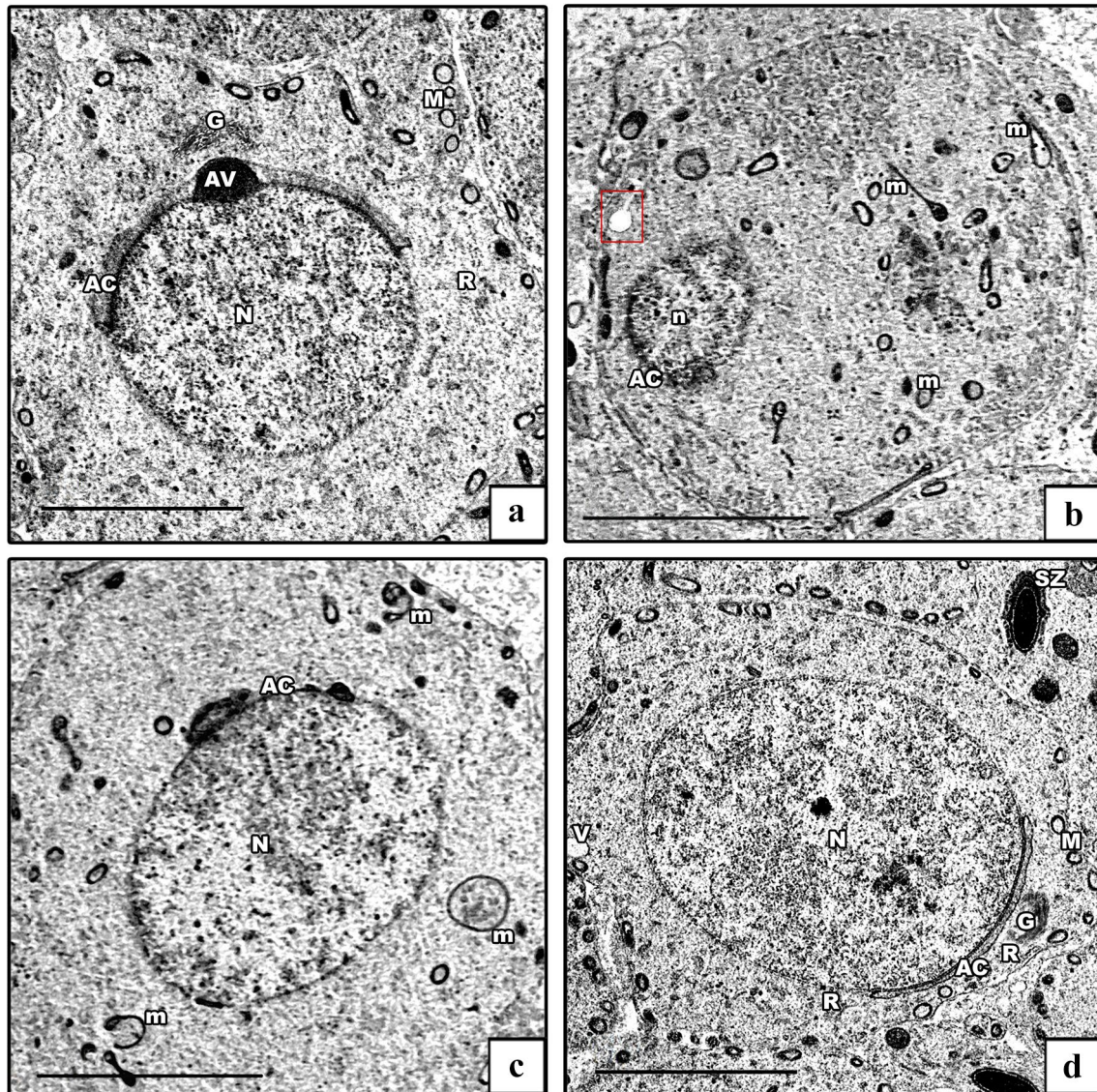
Fig. 11 Electron micrographs of rounded spermatid. **a** Control group demonstrates a rounded spermatid with a spherical euchromatic nucleus (N) with a prominent acrosomal cap (AC) and an acrosomal vesicle (AV). Its cytoplasm shows a well-developed Golgi apparatus (G), rER (R), and mitochondria (M). **b**, **c** AlCl₃ group. **b** Degenerated rounded spermatid with a shrunken heterochromatic nucleus (n) and abnormal acrosomal cap (AC) are seen. Its cytoplasm shows a swollen rER (red box) and vacuolated mitochondria (m). **c** Early sper- matid with an euchromatic nucleus (N) and ill-developed acrosomal cap (AC) are seen. Its cytoplasm shows vacuolated and ring-shaped mitochondria (m). **d** AlCl₃ plus taurine group: normally rounded spermatid with a spherical euchromatic nucleus (N) with prominent acrosomal cap (AC). The cytoplasm shows a well-developed Golgi apparatus (G), normal rER (R), mitochondria (M), and some vacuoles (V). Note the presence of spermatozoa (SZ). Transmission electron microscope, scale bars = 5 μm (**a**–**d**)

distortion and dysfunction induced by AlCl₃ administration via damping mitochondrial damage and ER stress.

Taurine significantly restored the architecture of testes, epididymis, spermatogonia, spermatids, and spermatozoa. This could be explained by the antioxidant effect of tau- rine, emphasized by the decreased MDA and increased TAC seen in the current study. Our results are in accord- ance with the findings of Adedara et al. (2018). Moreover, Adedara and colleagues reported that taurine considerably

increased the testicular and epididymal sperm counts and progressive motility. Besides, taurine restored the marker enzymes of testicular function, specifically acid and alkaline phosphatases and lactate dehydrogenase, and conserved the standard ultrastructural features of the testis and epididymis (Adedara et al. 2018). Taurine induced gene expression of the antioxidant nuclear factor (erythroid-derived 2)-like2 (*Nrf2*), glutathione peroxidase-1 (*GPX-1*), and heme oxy- genase-1 (*HO-1*) and enhanced the activities of glutathione
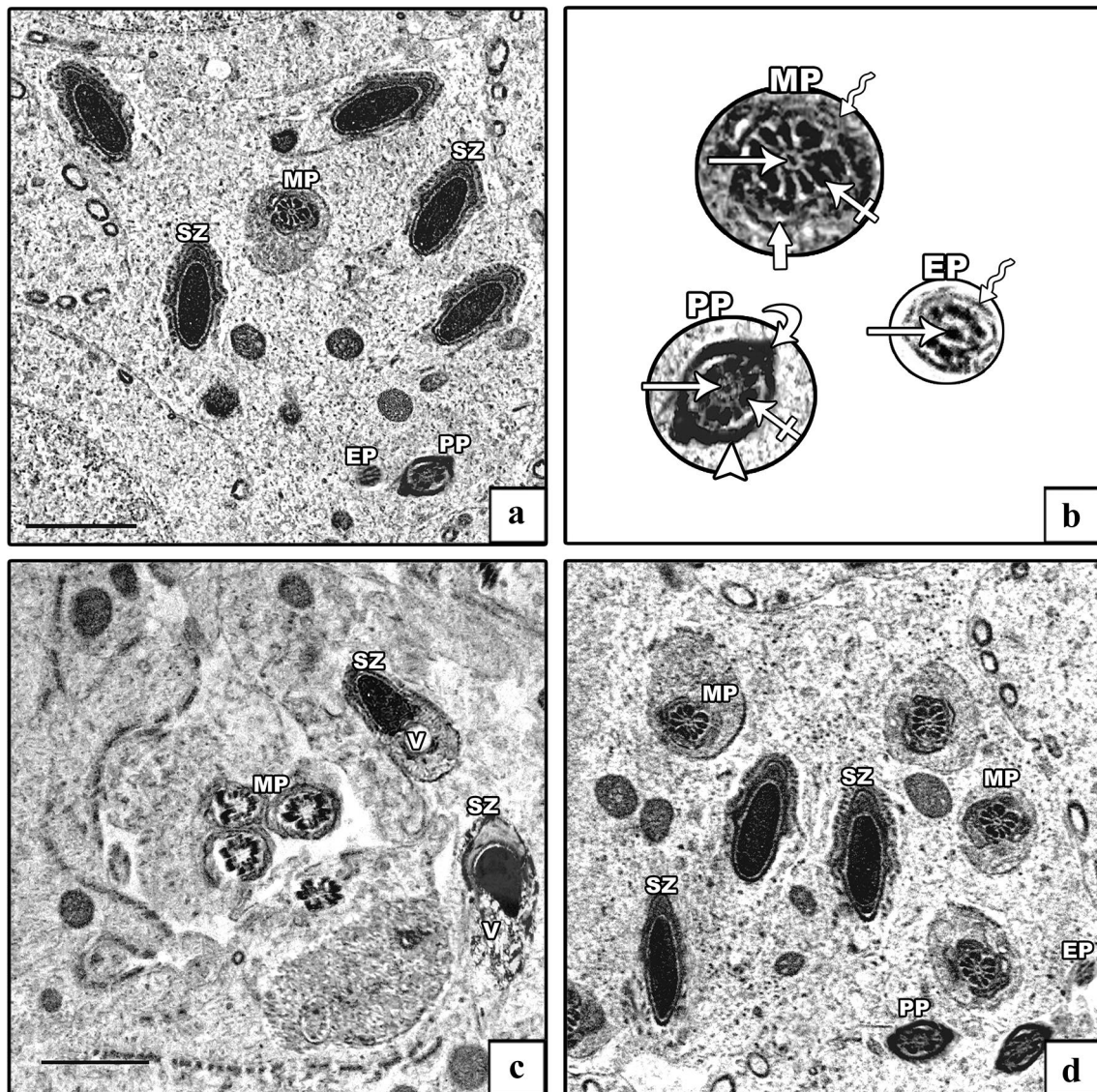
Fig. 12 Electron micrographs of spermatozoa. **a**, **b** Control group shows the spermatozoa head with an elongated electron-dense nucleus (SZ). The tail has its middle piece (MP), principal piece (PP), and end piece (EP). The middle piece comprises (from inside to out) central axoneme (arrow), nine outer dense fibers (crossed arrow), mitochondrial sheath (thick arrow), and plasma membrane (zigzag arrow). The principal piece comprises a central axoneme (arrow), nine outer dense fibers (crossed arrow), and two longitudinal columns (curved arrow) connected by transverse circumferential ribs (arrow-head). The end piece comprises the central axoneme (arrow) and plasma membrane (zigzag arrow). **c** AlCl₃ group: degenerated head of spermatozoa (SZ) with vacuolation in its retained cytoplasm (V) is seen with abnormal outlines and incomplete mitochondrial sheath of the middle piece (MP). **d** AlCl₃ plus taurine group exhibits a normal picture of the spermatozoa head (SZ) as well a middle piece (MP), principal piece (PP), and end piece (EP) of the tail. Transmission electron microscope, scale bars = 2 μm (**a**, **c**, **d**)

(GSH) and GPX, resulting in a decline of the MDA content and improvement of the cellular TAC (Agca et al. 2014; Han et al. 2020).

The antiapoptotic effect of taurine was emphasized by a decrease in *Bax* expression and immunoreactivity with a concomitant increase in *Bcl-2* gene expression in taurine-treated rats in this study. These findings were in agreement with the results of Yang et al. (2015). Sedaghat (2021) stated that taurine exerts its antiapoptotic effect by inhibiting the

mitochondrial pathway and reverting the gene expression of *Bax/Bcl-2* to normal, as reported herein. Besides, caspase-3 and caspase-9 were also inhibited by taurine (Madbouly et al. 2021).

Taurine is a component of the mitochondrial tRNAs, as two taurine-containing modified uridines were identified. Taurine-conjugated uridines are linked to the role of taurine as an antioxidant (Jong et al. 2021). The antioxidant effect of taurine is associated with an improvement of

the mitochondrial function, as it stimulates the mitochondrial protein synthesis and enhances the activity of the electron transfer chain (Bhattacharjee et al. 2021). Also, taurine regulates the intracellular calcium homeostasis, hence protecting against glutamate-induced mitochondrial damage and cell death (Baliou et al. 2021), in addition to its role in the inhibition of mitochondria-mediated apoptosis (Jong et al. 2017), as discussed above.

Taurine prevents the abnormal increase in the mitochondrial calcium level, inhibits the mitochondrial membrane depolarization, protects against the mitochondrial

Fig. 14 Histomorphomertic, biochemical, and molecular parameters of testes of all studied groups. **a** Area percent of Bax immunoreaction. **b** Area percent of vimentin immunoreaction. **c** Leydig cell (count/100 μm^2). **d** MDA (nmol/g tissue). **e** TAC (ng/mg protein). **f** *Vimentin* gene expression ($2^{-\Delta\Delta CT}$). **g** *Bax* gene expression ($2^{-\Delta\Delta CT}$). **h** *Bcl-2* gene expression ($2^{-\Delta\Delta CT}$). **i** *PCNA* gene expression ($2^{-\Delta\Delta CT}$). **J** *XBP1* gene expression ($2^{-\Delta\Delta CT}$). **K** *CHOP* gene expression ($2^{-\Delta\Delta CT}$). Data presented as mean ± SD. Statistically significant: *$p < 0.05$ and ***$p < 0.0001$

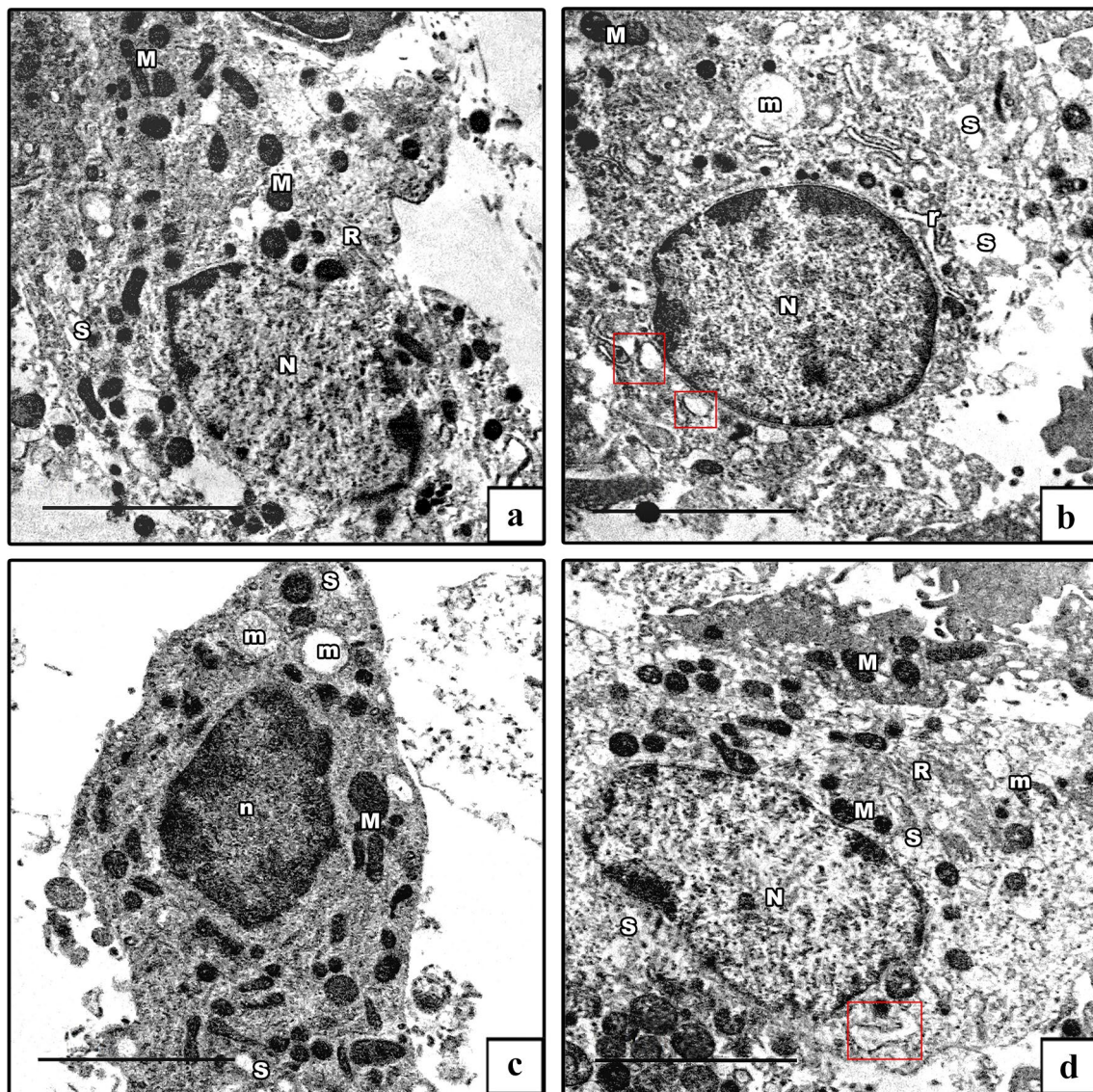dysfunction and cell damage (Jong et al. 2021), and regulates the energy metabolism (Lan et al. 2021). Moreover,

Fig. 13 Electron micrographs of Leydig cells. **a** Control group demonstrates Leydig cells with an oval euchromatic nucleus (N), sER (S), rER (R), and mitochondria (M). **b, c** AlCl₃ group: degenerated Leydig cells. Some cells have irregular nuclei (N), and others have shrunken heterochromatic nuclei (PN). The cytoplasm reveals dilated sER (s), dilated rER (r), swollen rER (red box), normal mitochondria (M), and vacuolated ones (m) **d** AlCl₃ plus taurine group shows normal Leydig cells with normal mitochondria (M) and normal rER (R) apart from some dilated rER (red box) and some vacuolated mitochondria (m). Transmission electron microscope, scale bars = 5 μm (**a–d**)
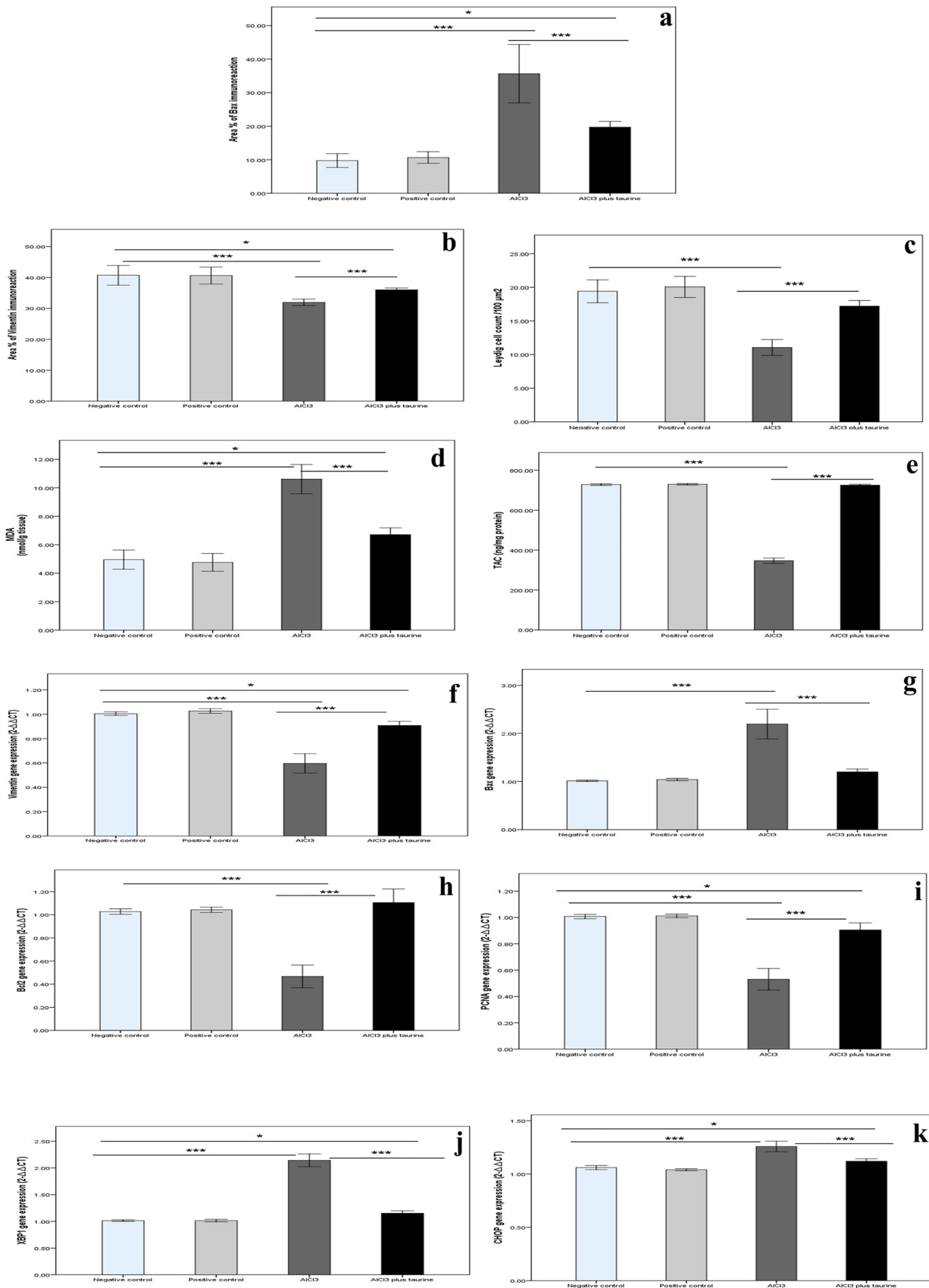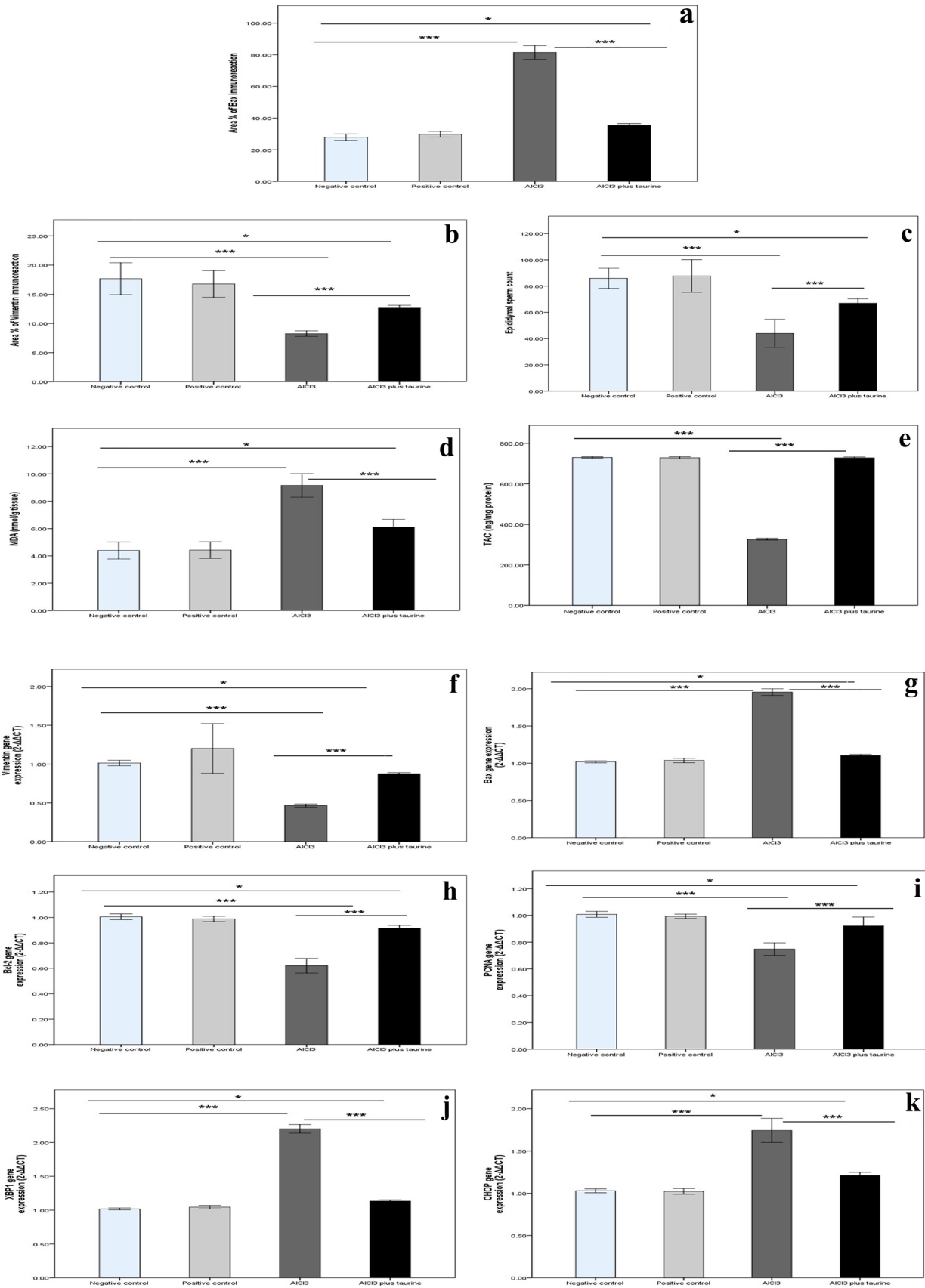
◀**Fig. 15** Histomorphometric, biochemical, and molecular parameters of epididymis of all studied groups. **a** Area percent of Bax immunoreaction. **b** Area percent of vimentin immunoreaction. **c** Epididymal sperm count (million/ml). **d** MDA (nmol/g tissue). **e** TAC (ng/mg protein). **f** *Vimentin* gene expression ($2^{-\Delta\Delta CT}$). **g** *Bax* gene expression ($2^{-\Delta\Delta CT}$). **h** *Bcl-2* gene expression ($2^{-\Delta\Delta CT}$). **i** *PCNA* gene expression ($2^{-\Delta\Delta CT}$). **J** *XBP1* gene expression ($2^{-\Delta\Delta CT}$). **K** *CHOP* gene expression ($2^{-\Delta\Delta CT}$). Data presented as mean $\pm$ SD. Statistically significant: *$p < 0.05$ and ***$p < 0.0001$

taurine is capable of improving ER homeostasis, and limiting the inflammatory reaction (Stacchiotti et al. 2018). Taurine reduces the apoptosis induced by oxidative free radicals related to ER stress, as it regulates the expression of *XBP1* and other related ER stress genes such as *ATF4* and *CHOP* (Men et al. 2010). These findings are confirmed in the current study by the significant decrease in *XBP1* and *CHOP* gene expression. Taurine also suppresses two of the three UPR pathways as it can improve protein folding by reducing oxidative stress and providing a better osmotic environment for protein folding (Schaffer and Kim 2018).

These taurine-specific mechanisms, together with their detection in the seminal fluid, gonadal vascular endothelial, germinal, and Leydig cells, besides the covering epithelium of efferent gonadal ducts (Rezaee-Tazangi et al. 2020), prove it to be a candidate for protection of gonads from AlCl$_3$-induced damage. Moreover, Rezaee-Tazangi et al. (2020) reported that taurine improved the viability, motility, and progressive movement velocity of sperm by suppressing cell death signaling.

Also, taurine displayed a proliferative-inducing effect on testes and epididymis, as confirmed by the highly expressed *PCNA*. These results supported the findings of Liu et al. (2015), who stated that antenatal taurine supplementation increased *PCNA* mRNA expression and the markedly increased PCNA-positive cell counts in intrauterine growth restriction of fetal rat brain tissues improved neuronal regeneration.

In conclusion, oxidative-stress-induced mitochondrial injury and ER stress were fundamental pathophysiological mechanisms that could explain the damaging effect of AlCl$_3$ on male gonads. This effect was confirmed by the evident ultrastructural impairment visualized by light and EM examinations of both testicular and epididymal tissues. These findings could be explained by the disturbed gene expression of apoptotic and ER stress markers at the molecular level and the increased oxidative stress markers at the biochemical level. Moreover, taurine supplementation was associated with marked improvement of oxidative stress, mitochondrial injury, ER stress, and apoptotic markers, as evident from the restoration of the standard architecture of both testicular and epididymal tissues. Overall, the results of this study highlight the beneficial

effects and mechanisms of action of taurine in the reproductive system of an AlCl$_3$-induced gonadal damage rat model. Accordingly, taurine supplementation may be a hopeful natural therapeutic regimen with fewer adverse effects that could be used to inhibit or counteract male reproductive insufficiency.

Data availability Raw data related to the current study are available from the corresponding author upon reasonable request.

Declarations

Conflict of interest All authors declare no conflicts.

Ethical approval Ethical committee approval IP (IRP no. 00012098-FWA NO:00018699).

References

Abdel-Moneim AM (2013) Effects of taurine against histomorphological and ultrastructural changes in the testes of mice exposed to aluminium chloride. Arh Hig Rada Toksikol 64:3. https://doi.org/10.2478/10004-1254-64-2013-2322

Aboelwafa HR, El-Kott AF, Abd-Ella EM, Yousef HN (2020) The possible neuroprotective effect of silymarin against aluminum chloride-prompted Alzheimer's-like disease in rats. Brain Sci 10:628. https://doi.org/10.3390/brainsci10090628

Adedara IA, Alake SE, Adeyemo MO, Olajide LO, Ajibade TO, Farombi EO (2018) Taurine enhances spermatogenic function and antioxidant defense mechanisms in testes and epididymis of L-NAME-induced hypertensive rats. Biomed Pharmacother 97:181–189. https://doi.org/10.1016/j.biopha.2017.10.095

Agarwal A, Sengupta P (2020) Oxidative stress and its association with male infertility. In: Male infertility. Springer, Cham, pp 57–68

Agca CA, Tuzcu M, Hayirli A, Sahin K (2014) Taurine ameliorates neuropathy via regulating NF-κB and Nrf2/HO-1 signaling cascades in diabetic rats. Food Chem Toxicol 71:116–121. https://doi.org/10.1016/j.fct.2014.05.023

Ahmadian M, Roshan VD, Aslani E, Stannard SR (2017) Taurine supplementation has anti-atherogenic and anti-inflammatory effects before and after incremental exercise in heart failure. Ther Adv Cardiovasc Dis 11:185–194. https://doi.org/10.1177/1753944717711138

Ahmed SA, Mohammed WI (2021) Carvedilol induces the antiapoptotic proteins Nrf2 and Bcl2 and inhibits cellular apoptosis in aluminum-induced testicular toxicity in male Wistar rats. Biomed Pharmacother 139:111594. https://doi.org/10.1016/j.biopha.2021.111594

Akinola BK, Olawuyi TS, Ukwenya VO, Daniel LD, Faleye BC (2021) Protective effects of aloe vera gel (*Aloe baberdensis* Miller) on aluminum chloride-induced reproductive toxicity in male wistar rats. JBRA Assist Reprod 25:193–201. https://doi.org/10.5935/1518-0557.20200082

Alam MS, Kurohmaru M (2014) Disruption of Sertoli cell vimentin filaments in prepubertal rats: an acute effect of butylparaben in vivo and in vitro. Acta Histochem 116:682–687. https://doi.org/10.1016/j.acthis.2013.12.006

Alasmari W, Faruk E, Abourehab M, Elshazly A, El Sawy N (2018) The effect of metformin versus vitamin e on the testis of adult diabetic albino rats: histological, biochemical and immunohistochemistry study. Arsci 6:113–132. https://doi.org/10.4236/arsci.2018.64010

Alghamdi BS (2018) Possible prophylactic anti-excitotoxic and anti-oxidant effects of virgin coconut oil on aluminium chloride-induced Alzheimer's in rat models. J Integr Neurosci 17:593–607. https://doi.org/10.3233/JIN-180089

Al-Kahtani MA (2010) Renal damage mediated by oxidative stress in mice treated with aluminium chloride: protective effects of taurine. J Biol Sci 10:584–595. https://doi.org/10.3923/jbs.2010.584.595

Al-Megrin WA, Alomar S, Alkhuriji AF, Metwally DM, Mohamed SK, Kassab RB, Abdel Moneim AE, El-Khadragy MF (2020) Luteolin protects against testicular injury induced by lead acetate by activating the Nrf2/HO-1 pathway. IUBMB Life 72:1787–1798. https://doi.org/10.1002/iub.2311

ALMurshidi MM, Raheem SA, Razaq RA (2021) Some histological and physiological effects of aluminum chloride on some reproductive organs of male albino mice (Musmusculus). Ann RSCB 25:5906–5918

Al-Otaibi SS, Arafah MM, Sharma B, Alhomida AS, Siddiqi NJ (2018) Synergistic effect of quercetin and α-lipoic acid on aluminium chloride induced neurotoxicity in rats. J Toxicol 2018:2817036. https://doi.org/10.1155/2018/2817036

Arab-Nozari M, Zamani E, Latifi A, Shaki F (2019) Mitochondrial toxicity of aluminium nanoparticles in comparison to its ionic form on isolated rat brain mitochondria. Bratisl Lek Listy 120:516–522. https://doi.org/10.4149/BLL_2019_083

Asadi N, Bahmani M, Kheradmand A, Rafieian-Kopaei M (2017) The impact of oxidative stress on testicular function and the role of antioxidants in improving it: a review. J Clin Diagn Res. https://doi.org/10.7860/JCDR/2017/23927.9886

Baliou S, Adamaki M, Ioannou P, Pappa A, Panayiotidis MI, Spandidos DA, Christodoulou I, Kyriakopoulos AM, Zoumpourlis V (2021) Protective role of taurine against oxidative stress. Mol Med Rep 24:1–19. https://doi.org/10.3892/mmr.2021.12242

Bancroft JD, Gamble M (2008) Theory and Practice of Histological Techniques, 6th edn. Churchill Livingstone, Elsevier, China

Barati E, Nikzad H, Karimian M (2020) Oxidative stress and male infertility: current knowledge of pathophysiology and role of antioxidant therapy in disease management. Cell Mol Life Sci 77:93–113. https://doi.org/10.1007/s00018-019-03253-8

Berihu BA (2015) Histological and functional effect of aluminium on male reproductive system. Int J Pharm Sci Res 6:1122–1132

Bhat MA, Ahmad K, Khan MS, Bhat MA, Almatroudi A, Rahman S, Jan AT (2020) Expedition into taurine biology: structural insights and therapeutic perspective of taurine in neurodegenerative diseases. Biomolecules 10:863. https://doi.org/10.3390/biom10060863

Bhattacharjee A, Prajapati SK, Krishnamurthy S (2021) Supplementation of taurine improves ionic homeostasis and mitochondrial function in the rats exhibiting post-traumatic stress disorder-like symptoms. Eur J Pharmacol 908:174361. https://doi.org/10.1016/j.ejphar.2021.174361

Bonora M, Patergnani S, Ramaccini D, Morciano G, Pedriali G, Kahsay AE, Bouhamida E, Giorgi C, Wieckowski MR, Pinton P (2020) Physiopathology of the permeability transition pore: molecular mechanisms in human pathology. Biomolecules 10:1–25. https://doi.org/10.3390/biom10070998

Cemek M, Kağa S, Şimşek N, Büyükokuroğlu ME, Konuk M (2008) Antihyperglycemic and antioxidative potential of matricaria chamomilla L. in streptozotocin-induced diabetic rats. J Nat Med 62:284–293. https://doi.org/10.1007/s11418-008-0228-1

Cheng X, Peuckert C, Wölfl S (2017) Essential role of mitochondrial Stat3 in P38MAPK mediated apoptosis under oxidative stress. Sci Rep 7:1–11. https://doi.org/10.1038/s41598-017-15342-4

Chianese R, Pierantoni R (2021) Mitochondrial reactive oxygen species (ROS) production alters sperm quality. Antioxidants (Basel) 10:1–19. https://doi.org/10.3390/antiox10010092

Chiu WT, Chang HA, Lin YH, Lin YS, Chang HT, Lin HH, Huang SC, Tang MJ, Shen MR (2018) Bcl-2 regulates store-operated Ca^{2+} entry to modulate ER stress-induced apoptosis. Cell Death Discov 4:1–14. https://doi.org/10.1038/s41420-018-0039-4

Dera HA, Abushouk A (2015) Protective effect of resveratrol against aluminium chloride (ALCL3) induced testicular damage in rats entails inhibition of intrinsic apoptotic pathway. Sci Adv Mater 7:384–395. https://doi.org/10.1166/sam.2015.2250

Draper HH, Squires EJ, Mahmoodi H, Wu J, Agarwal S, Hadley MA (1993) A comparative evaluation of thiobarbituric acid methods for the determination of malondialdehyde in biological materials. Free Radic Biol Med 15:353–363. https://doi.org/10.1016/0891-5849(93)90035-s

Duan Y, Li J, Jing X, Ding X, Yu Y, Zhao Q (2020) Fucoidan induces apoptosis and inhibits proliferation of hepatocellular carcinoma via the P38 MAPK/ERK and PI3K/Akt signal pathways. Cancer Manag Res 12:1713. https://doi.org/10.2147/CMAR.S243495

Durairajanayagam D, Singh D, Agarwal A, Henkel R (2021) Causes and consequences of sperm mitochondrial dysfunction. Andrologia 53:e13666. https://doi.org/10.1111/and.13666

Dutta S, Sengupta P, Slama P, Roychoudhury S (2021) Oxidative stress, testicular inflammatory pathways, and male reproduction. Int J Mol Sci 22:1–20. https://doi.org/10.3390/ijms221810043

El-Gayar HA, El-Habibi EM, Edrees GM, Salem ET, Gouida MS (2016) Role of alcoholic extracts of *Eruca sativa* or *Petroselinum crispum* on dioxin-induced testicular oxidative stress and apoptosis. Int J Sci Res 5:1415–1421

Fang F, Ni K, Cai Y, Zhao Q, Shang J, Zhang X, Shen S, Xiong C (2017) Busulfan administration produces toxic effects on epididymal morphology and inhibits the expression of ZO-1 and vimentin in the mouse epididymis. Biosci Rep 37:1–12. https://doi.org/10.1042/BSR20171059

Ghoneim FM, Khalaf HA, Elsamanoudy AZ, Helaly AN (2014) Effect of chronic usage of tramadol on motor cerebral cortex and testicular tissues of adult male albino rats and the effect of its

withdrawal: histological, immunohistochemical and biochemical study. Int J Clin Exp Pathol 7:7323–7341

Ghoneim FM, Alrefai H, Elsamanoudy AZ, Abo El-khair SM, Khalaf HA (2020) The protective role of prenatal alpha lipoic acid supplementation against pancreatic oxidative damage in offspring of valproic acid-treated rats: histological and molecular study. Biology (Basel) 9:239. https://doi.org/10.3390/biology9090239

Giacomello M, Pyakurel A, Glytsou C, Scorrano L (2020) The cell biology of mitochondrial membrane dynamics. Nat Rev Mol Cell Biol 21:204–224. https://doi.org/10.1038/s41580-020-0210-7

Giménez-Cassina A, Danial NN (2015) Regulation of Mitochondrial nutrient and energy metabolism by BCL-2 family proteins. Trends Endocrinol Metab 26:165–175. https://doi.org/10.1016/j.tem.2015.02.004

Guo CH, Liao SY, Yuan CY, Hsu GS (2006) Effects of peritoneal aluminum overload on polyamines and nitric oxide contents of testes and epididymis in the mice. Environ Toxicol Pharmacol 21:1–7. https://doi.org/10.1016/j.etap.2005.03.010

Gupte R, Christian S, Keselman P, Habiger J, Brooks WM, Harris JL (2019) Evaluation of taurine neuroprotection in aged rats with traumatic brain injury. Brain Imaging Behav 13:461–471. https://doi.org/10.1007/s11682-018-9865-5

Güvenç M, Cellat M, Gökçek İ, Arkalı G, Uyar A, Tekeli İO, Yavaş İ (2020) Tyrosol prevents AlCl3 induced male reproductive damage by suppressing apoptosis and activating the Nrf-2/HO-1 pathway. Andrologia 52:e13499. https://doi.org/10.1111/and.13499

Han HL, Zhang JF, Yan EF, Shen MM, Wu JM, Gan ZD, Wei CH, Zhang LL, Wang T (2020) Effects of taurine on growth performance, antioxidant capacity, and lipid metabolism in broiler chickens. Poult Sci 99:5707–5717. https://doi.org/10.1016/j.psj.2020.07.020

Heinrich A, Potter SJ, Guo L, Ratner N, DeFalco T (2020) Distinct roles for Rac1 in Sertoli cell function during testicular development and spermatogenesis. Cell Rep 31:107513. https://doi.org/10.1016/j.celrep.2020.03.077

Hosseini M, Shaygannia E, Rahmani M, Eskandari A, Golsefid AA, Tavalaee M, Gharagozloo P, Drevet JR, Nasr-Esfahani MH (2020) Endoplasmic reticulum stress (ER Stress) and unfolded protein response (UPR) occur in a rat varicocele testis model. Oxid Med Cell Longev 2020:5909306. https://doi.org/10.1155/2020/5909306

Huo R, Zhu YF, Ma X, Lin M, Zhou ZM, Sha JH (2004) Differential expression of glucose-regulated protein 78 during spermatogenesis. Cell Tissue Res 316:359–367. https://doi.org/10.1007/s00441-004-0885-7

Ibrahim AA, Karam HM, Shaaban EA, Safar MM, El-Yamany MF (2019) MitoQ ameliorates testicular damage induced by gamma irradiation in rats: modulation of mitochondrial apoptosis and steroidogenesis. Life Sci 232:116655. https://doi.org/10.1016/j.lfs.2019.116655

Idari G, Karimi P, Ghaffari S, Hashemy SI, Mashkani B (2021) Protective effects of BiP inducer X (BIX) against diabetic cardiomyopathy in rats. Can J Physiol Pharmacol 99:1–10. https://doi.org/10.1139/cjpp-2020-0419

Igbokwe IO, Igwenagu E, Igbokwe NA (2019) Aluminium toxicosis: a review of toxic actions and effects. Interdiscip Toxicol 12:45. https://doi.org/10.2478/intox-2019-0007

Iglesias-González J, Sánchez-Iglesias S, Beiras-Iglesias A, Méndez-Álvarez E, Soto-Otero R (2017) Effects of aluminium on rat brain mitochondria bioenergetics: an in vitro and in vivo study. Mol Neurobiol 54:563–570. https://doi.org/10.1007/s12035-015-9650-z

Ito T, Schaffer SW, Azuma J (2012) The potential usefulness of taurine on diabetes mellitus and its complications. Amino Acids 42:1529–1539. https://doi.org/10.1007/s00726-011-0883-5

Ito T, Yoshikawa N, Ito H, Schaffer SW (2015) Impact of taurine depletion on glucose control and insulin secretion in mice. J Pharmacol Sci 129:59–64. https://doi.org/10.1016/j.jphs.2015.08.007

Jong CJ, Ito T, Prentice H, Wu JY, Schaffer SW (2017) Role of mitochondria and endoplasmic reticulum in taurine-deficiency-mediated apoptosis. Nutrients 9:795. https://doi.org/10.3390/nu9080795

Jong CJ, Sandal P, Schaffer SW (2021) The role of taurine in mitochondria health: more than just an antioxidant. Molecules 26:4913. https://doi.org/10.3390/molecules26164913

Jurkowska K, Kratz EM, Sawicka E, Piwowar A (2019) The impact of metalloestrogens on the physiology of male reproductive health as a current problem of the XXI century. J Physiol Pharmacol 70:337–355. https://doi.org/10.26402/jpp.2019.3.02

Kalaiselvi A, Suganthy OM, Govindassamy P, Vasantharaja D, Gowri B, Ramalingam V (2014) Influence of aluminium chloride on antioxidant system in the testis and epididymis of rats. Iranian J Toxicol 8:991–997

Karna K, Choi B, Lee S, Kim C, Shin Y, Yang S, Moon K, Hyun J, Park K, Park J (2019) DA-9401 Attenuates adriamycin-induced testicular toxicity in Sprague-Dawley rats. BJU Int 123:51

Karna KK, Shin YS, Choi BR, Kim HK, Park JK (2019b) The role of endoplasmic reticulum stress response in male reproductive physiology and pathology: a review. World J Mens Health 37:484–494. https://doi.org/10.5534/wjmh.190038

Khafaga AF (2017) Exogenous phosphatidylcholine supplementation retrieve aluminum-induced toxicity in male albino rats. Environ Sci Pollut Res Int 24:15589–15598. https://doi.org/10.1007/s11356-017-9151-x

Khalaf HA, El-Mansy AAE (2019) The possible alleviating effect of saffron on chlorpyrifos experimentally induced cardiotoxicity: Histological, immunohistochemical and biochemical study. Acta Histochem 121:472–483. https://doi.org/10.1016/j.acthis.2019.03.003

Kim S, Joe Y, Kim HJ, Kim YS, Jeong SO, Pae HO, Ryter SW, Surh YJ, Chung HT (2015) Endoplasmic reticulum stress-induced IRE1α activation mediates cross-talk of GSK-3β and XBP-1 to regulate inflammatory cytokine production. J Immunol 194:4498–4506. https://doi.org/10.4049/jimmunol.1401399

Koppers AJ, De Iuliis GN, Finnie JM, McLaughlin EA, Aitken RJ (2008) Significance of mitochondrial reactive oxygen species in the generation of oxidative stress in spermatozoa. J Clin Endocrinol Metab 93:3199–3207. https://doi.org/10.1210/jc.2007-2616

Lan R, Wan Z, Xu Y, Wang Z, Fu S, Zhou Y, Lin X, Han X, Luo Z, Miao J, Yin Y (2021) Taurine reprograms mammary-gland metabolism and alleviates inflammation induced by Streptococcus uberis in mice. Front Immunol 12:2197. https://doi.org/10.3389/fimmu.2021.696101

Landau S, Everitt BS (2003) A handbook of statistical analyses using SPSS. Chapman and Hall/CRC

Li Y, Guo Y, Tang J, Jiang J, Chen Z (2014) New insights into the roles of CHOP-induced apoptosis in ER stress. Acta Biochim Biophys Sin (Shanghai) 46:629–640. https://doi.org/10.1093/abbs/gmu048

Liu J, Wang HW, Liu F, Wang XF (2015) Antenatal taurine improves neuronal regeneration in fetal rats with intrauterine growth restriction by inhibiting the Rho-ROCK signal pathway. Metab Brain Dis 30:67–73. https://doi.org/10.1007/s11011-014-9572-x

Liu H, Zhang W, Fang Y, Yang H, Tian L, Li K, Lai W, Bian L, Lin B, Liu X, Xi Z (2020) Neurotoxicity of aluminum oxide nanoparticles and their mechanistic role in dopaminergic neuron injury involving P53-related pathways. J Hazard Mater 392:122312. https://doi.org/10.1016/j.jhazmat.2020.122312

Lokman M, Ashraf E, Kassab RB, Abdel Moneim AE, El-Yamany NA (2021) Aluminum chloride-induced reproductive toxicity in rats: the protective role of zinc oxide nanoparticles. Biol Trace Elem Res. https://doi.org/10.1007/s12011-021-03010-8

Lu J, Huang Q, Zhang D, Lan T, Zhang Y, Tang X, Xu P, Zhao D, Cong D, Zhao D, Sun L (2020) The protective effect of DiDang tang against AlCl₃-induced oxidative stress and apoptosis in PC12 cells through the activation of SIRT1-mediated Akt/Nrf2/HO-1 pathway. Front Pharmacol 11:466. https://doi.org/10.3389/fphar.2020.00466

Madbouly N, Azmy A, Salama A, El-Amir A (2021) The nephroprotective properties of taurine-amikacin treatment in rats are mediated through HSP25 and TLR-4 regulation. J Antibiot (Tokyo) 74:580–592. https://doi.org/10.1038/s41429-021-00441-2

Marcinkiewicz J, Kontny E (2014) Taurine and inflammatory diseases. Amino Acids 46:7–20. https://doi.org/10.1007/s00726-012-1361-4

Men X, Han S, Gao J, Cao G, Zhang L, Yu H, Lu H, Pu J (2010) Taurine protects against lung damage following limb ischemia reperfusion in the rat by attenuating endoplasmic reticulum stress-induced apoptosis. Acta Orthop 81:263–267. https://doi.org/10.3109/17453671003587085

Moustafa AE, Amr IM, Gebaly ZM (2012) Evaluation the effect of sildenafil citrate (SC or Viagra) on senile albino rat testis (histological and biochemical study). Egypt J Hosp Med 49:911–932. https://doi.org/10.21608/EJHM.2012.16227

Nguyen TM, Vegrichtova M, Tlapakova T, Krulova M, Krylov V (2019) The Interconnection between cytokeratin and cell membrane-bound β-catenin in Sertoli cells derived from juvenile *Xenopus tropicalis* testes. Biol Open. https://doi.org/10.1242/bio.043950

Niu H, Ding S, Li H, Wei J, Ren C, Wu X, Huma T, Zhang Q (2018) Effect of long-term sodium salicylate administration on learning, memory, and neurogenesis in the rat hippocampus. Biomed Res Int. https://doi.org/10.1155/2018/7807426

Nna VU, Udefa AL, Ofutet EO, Osim EE (2017) Testicular and epididymal histology of rats chronically administered high doses of phosphodiesterase-5 inhibitors and tramadol. Niger J Physiol Sci 32:55–61

Nuhair R (2015) Effects of aluminum chloride on some hormones levels and reproductive organs of male rats (*Rattus norvegicus*). J Thi-Qar Sci 5:3–8

Oja SS, Saransaari P (2013) Taurine and epilepsy. Epilepsy Res 104:187–194. https://doi.org/10.1016/j.eplepsyres.2013.01.010

Okail HA, Ibrahim AS, Badr AH (2020) The protective effect of propolis against aluminum chloride-induced hepatorenal toxicity in albino rats. JoBAZ 81:34. https://doi.org/10.1186/s41936-020-00169-9

Panahi S, Karamian A, Sajadi E, Aliaghaei A, Nazarian H, Abdi S, Danyali S, Paktinat S, Abdollahifar MA, Farahani RM (2020) Sertoli cell – conditioned medium restores spermatogenesis in azoospermic mouse testis. Cell Tissue Res 379:577–587. https://doi.org/10.1007/s00441-019-03092-w

Pandey G, Jain GC (2013) A review on toxic effects of aluminium exposure on male reproductive system and probable mechanisms of toxicity. Int J Toxicol Appl Pharmacol 3:48–57

Promyo K, Iqbal F, Chaidee N, Chetsawang B (2020) Aluminum chloride-induced amyloid β accumulation and endoplasmic reticulum stress in rat brain are averted by melatonin. Food Chem Toxicol 146:111829. https://doi.org/10.1016/j.fct.2020.111829

Qaradakhi T, Gadanec LK, McSweeney KR, Abraham JR, Apostolopoulos V, Zulli A (2020) The anti-inflammatory effect of taurine on cardiovascular disease. Nutrients 12:2847. https://doi.org/10.3390/nu12092847

Reichert KP, Bottari NB, Schetinger MR, da Silva AD, Assmann CE, da Costa P, Lopes TF, Heidrich G, Dressler V, Morsch VM (2021) Aluminum chloride impairs learning and memory by P2X7 and A2A-receptor stimulations in hippocampus of mice. PhD diss, Universidade Federal de Santa Maria. https://doi.org/10.21203/rs.3.rs-329182/v1

Rezaee-Tazangi F, Zeidooni L, Rafiee Z, Fakhredini F, Kalantari H, Alidadi H, Khorsandi L (2020) Taurine effects on bisphenol A-induced oxidative stress in the mouse testicular mitochondria and sperm motility. JBRA Assist Reprod 24:428–435. https://doi.org/10.5935/1518-0557.20200017

Rikimaru M, Ohsawa Y, Wolf AM, Nishimaki K, Ichimiya H, Kamimura N, Nishimatsu S, Ohta S, Sunada Y (2012) Taurine ameliorates impaired the mitochondrial function and prevents stroke-like episodes in patients with MELAS. Intern Med 51:3351–3357. https://doi.org/10.2169/internalmedicine.51.7529

Saad HA, Hassieb MM, Oda SS, Tohamy HG, Khafaga AF (2018) Histopathologic study on the toxic effect of aluminium chloride on the heart, liver and kidneys of rabbits. AJVS 56:102–109. https://doi.org/10.5455/ajvs.264783

Sabha M Jr, Emirandetti A, Cullheim S, De Oliveira AL (2008) MHC I expression and synaptic plasticity in different mice strains after axotomy. Synapse 62:137–148. https://doi.org/10.1002/syn.20475

Sagara M, Murakami S, Mizushima S, Liu L, Mori M, Ikeda K, Nara Y, Yamori Y (2015) Taurine in 24-h urine samples is inversely related to cardiovascular risks of middle aged subjects in 50 populations of the world. Adv Exp Med Biol 803:623–636. https://doi.org/10.1007/978-3-319-15126-7_50

Sano R, Reed JC (2013) ER stress-induced cell death mechanisms. Biochim Biophys Acta 1833:3460–3470. https://doi.org/10.1016/j.bbamcr.2013.06.028

Schaffer S, Kim HW (2018) Effects and mechanisms of taurine as a therapeutic agent. Biomol Ther (Seoul) 26:225. https://doi.org/10.4062/biomolther.2017.251

Schaffer SW, Jong CJ, Ito T, Azuma J (2014) Role of taurine in the pathologies of MELAS and MERRF. Amino Acids 46:47–56. https://doi.org/10.1007/s00726-012-1414-8

Sedaghat M (2021) Cardiac remodeling, apoptosis-related process (Bax, Bcl-2), and their ratio (Bax/Bcl-2) in cardiomyocytes of diabetic rats after combined exercise training and taurine supplementation. Comp Clin Path 30:801–810. https://doi.org/10.1007/s00580-021-03275-4

Shaw CA (2018) Aluminum as a CNS and immune system toxin across the life span. Adv Exp Med Biol 1091:53–83. https://doi.org/10.1007/978-981-13-1370-7_4

Shetewy A, Shimada-Takaura K, Warner D, Jong CJ, Mehdi AB, Alexeyev M, Takahashi K, Schaffer SW (2016) Mitochondrial defects associated with B-alanine toxicity: relevance to hyper-beta-alaninemia. Mol Cell Biochem 416:11–22. https://doi.org/10.1007/s11010-016-2688-z

Skalny A, Aschner M, Jiang Y, Gluhcheva Y, Tizabi Y, Lobinski R, Tinkov A (2021) Molecular mechanisms of aluminum neurotoxicity: update on adverse effects and therapeutic strategies. Adv Neurotoxicol 5:1–34. https://doi.org/10.1016/bs.ant.2020.12.001

Stacchiotti A, Favero G, Lavazza A, Monsalve M, Rodella LF, Rezzani R (2018) Taurine supplementation alleviates puromycin aminonucleoside damage by modulating endoplasmic reticulum stress and mitochondrial-related apoptosis in rat kidney. Nutrients 10:689. https://doi.org/10.3390/nu10060689

Terrill JR, Pinniger GJ, Graves JA, Grounds MD, Arthur PG (2016) Increasing taurine intake and taurine synthesis improves skeletal muscle function in the mdx mouse model for Duchenne muscular dystrophy. J Physiol 594:3095–3110. https://doi.org/10.1113/JP271418

Wang S, Binder P, Fang Q, Wang Z, Xiao W, Liu W, Wang X (2018) Endoplasmic reticulum stress in the heart: insights into

mechanisms and drug targets. Br J Pharmacol 175:1293–1304. https://doi.org/10.1111/bph.13888

Wenting L, Ping L, Haitao J, Meng Q, Xiaofei R (2014) Therapeutic effect of taurine against aluminum-induced impairment on learning, memory and brain neurotransmitters in rats. Neurol Sci 35:1579–1584. https://doi.org/10.1007/s10072-014-1801-x

Woods AE, Stirling JW (2018) Transmission electron microscopy. In: Bancroft's theory and practice of histological techniques, pp 434–475

Xu F, Liu Y, Zhao H, Yu K, Song M, Zhu Y, Li Y (2017) Aluminum chloride caused liver dysfunction and mitochondrial energy metabolism disorder in rat. J Inorg Biochem 174:55–62. https://doi.org/10.1016/j.jinorgbio.2017.04.016

Xu D, Liu L, Zhao Y, Yang L, Cheng J, Hua R, Zhang Z, Li Q (2020) Melatonin protects mouse testes from palmitic acid-induced lipotoxicity by attenuating oxidative stress and DNA damage in a SIRT1-dependent manner. J Pineal Res 69:1–20. https://doi.org/10.1111/jpi.12690

Yamori Y, Taguchi T, Hamada A, Kunimasa K, Mori H, Mori M (2010) Taurine in health and diseases: consistent evidence from experimental and epidemiological studies. J Biomed Sci 17:S6. https://doi.org/10.1186/1423-0127-17-S1-S6

Yang J, Zong X, Wu G, Lin S, Feng Y, Hu J (2015) Taurine increases testicular function in aged rats by inhibiting oxidative stress and apoptosis. Amino Acids 47:1549–1558. https://doi.org/10.1007/s00726-015-1995-0

Yang SH, He JB, Yu LH, Li L, Long M, Liu MD, Li P (2019) Protective role of curcumin in cadmium-induced testicular injury in mice by attenuating oxidative stress via Nrf2/ARE pathway. Environ Sci Pollut Res Int 26:34575–35583. https://doi.org/10.1007/s11356-019-06587-9

Young IS (2001) Measurement of total antioxidant capacity. J Clin Pathol 54:339. https://doi.org/10.1136/jcp.54.5.339

Zhang L, Yuan Y, Tong Q, Jiang S, Xu Q, Ding J, Zhang L, Zhang R, Zhang K (2016) Reduced plasma taurine level in Parkinson's disease: association with motor severity and levodopa treatment. Int J Neurosci 126:630–636. https://doi.org/10.3109/00207454.2015.1051046

Zhu XM, Yao FH, Yao YM, Dong N, Yu Y, Sheng ZY (2012) Endoplasmic reticulum stress and its regulator XBP-1 contributes to dendritic cell maturation and activation induced by high mobility group box-1 protein. Int J Biochem Cell Biol 44:1097–1105. https://doi.org/10.1016/j.biocel.2012.03.018

Zhuang J, Lu Q, Shen B, Huang X, Shen L, Zheng X, Huang R, Yan J, Guo H (2015) TGFβ1 secreted by cancer-associated fibroblasts induces epithelial-mesenchymal transition of bladder cancer cells through LncRNA-ZEB2NAT. Sci Rep 5:1–13. https://doi.org/10.1038/srep11924

Publisher's Note Springer Nature remains neutral with regard to jurisdictional claims in published maps and institutional affiliations.